Enhancing Rail Track Performance Using Recycled Rubber Energy Absorbing Grids: Laboratory and Field Evidence

Suwan Hettiyahandi[1], Buddhima Indraratna, Ph.D, F.ASCE[2*], Trung Ngo, Ph.D, M.ASCE[3], Yujie Qi, Ph.D, M.ASCE[4], Chathuri Arachchige, Ph.D[5]

[1]PhD Candidate, Transport Research Centre, School of Civil and Environmental Engineering, University of Technology Sydney, Ultimo NSW 2007, Australia.
Email: Suwan.Hettiyahandi@student.uts.edu.au

[2*]Distinguished Professor of Civil Engineering and Director of Transport Research Centre, University of Technology Sydney, Ultimo, NSW 2007, Australia.
Email: Buddhima.Indraratna@uts.edu.au (*Corresponding author)

[3]Senior lecturer, Transport Research Centre, School of Civil and Environmental Engineering, University of Technology Sydney, Ultimo, NSW 2007, Australia.
Email: Trung.Ngo@uts.edu.au

[4]Senior lecturer, Transport Research Centre, School of Civil and Environmental Engineering, University of Technology Sydney, Ultimo, NSW 2007, Australia.
Email: Yujie.Qi@uts.edu.au

[5]Postdoctoral Research Associate, Transport Research Centre, School of Civil and Environmental Engineering, University of Technology Sydney, Ultimo, NSW 2007, Australia
Email: Chathuri.Arachchige@uts.edu.au

Abstract: Rail tracks deteriorate over time due to dynamic wheel loads, a process which necessitates frequent and costly maintenance. This paper presents the results of laboratory and field tests on the application of a Recycled Rubber Energy Absorbing Grid (REAG), made from conveyor belts previously used in mining to enhance the performance of ballasted tracks. These rubber grids having square apertures made with a waterjet cutting technique, were evaluated under simulated cyclic loads from heavy, high-speed trains using a large-scale process simulation testing apparatus (PSTA). The laboratory data indicates that REAG significantly improves track performance by providing substantial energy absorption and enhanced particle interlocking. The test data also shows that REAGs reduce lateral displacement, settlement, and ballast breakage, as well as enhance the resilient track modulus (M_{RT}) and energy dissipation per load cycle (E_d) of the track. Empirical models were then developed and calibrated with the laboratory results to predict the M_{RT} and cumulative energy dissipation after 250,000 cycles considering the role of REAG under cyclic loading. To validate the effectiveness of REAG in real-world conditions, a fully instrumented track section was constructed at Chullora, NSW, Australia. Field testing demonstrated that REAG placed underneath the ballast layer reduced settlement (by 18.3%) and vertical stress (up to 27%) in the sleeper-ballast and ballast-capping interfaces, as well as the acceleration measured on the sleepers, providing a promising solution to reduce the noise and vibration of railway tracks.

Key Words: recycled rubber grid, railway tracks, large-scale laboratory tests, field tests, energy absorption

Introduction

Railways play a crucial role in the transportation sector worldwide, both for passenger and freight services. With the current surge in population and urban expansion, heightened road traffic congestion and the increasing need for energy sources like fuel, railway industries are compelled to develop high-speed and heavy-duty rail routes to provide cost-efficient transportation solutions (Correia et al., 2016). However, traditional ballasted tracks require design enhancements to handle the increased stresses caused by rail traffic with greater axle loads (Arulrajah et al., 2009). Ballast provides a foundation for the tracks, stabilizes the substructure by distributing the load from moving trains and also improves drainage efficiency. Over time the dynamic stresses from train traffic progressively deteriorate the ballast layer, leading to substantial track settlement, buckling, instability, damage to track components, necessitating more frequent maintenance (Selig & Waters, 1994). For instance, the annual cost of maintaining ballasted rail tracks in New South Wales, Australia, is estimated at about 14-15 million dollars (Navaratnarajah & Indraratna, 2017), while ballast tamping and surface alignment in the U.S. costs roughly \$3,800 per kilometer (Chrismer & Davis, 2000). Consequently, reducing ballast degradation is crucial for improving the load-bearing capacity of the track substructure, lowering maintenance costs, and extending the operational lifespan of railway systems.

Over the past four decades, conventional polymer geogrids have been used to strengthen ballasted rail tracks (Bathurst & Raymond, 1987; Göbel et al., 1994; Horníček et al., 2010; Hussaini et al., 2015; Indraratna et al., 2019). While geogrids reduce lateral and vertical deformation and increase track stability and durability (Indraratna et al., 2013), polymer geogrids may rupture under high tensile stress and lose their reinforcing effect (Hatami et al., 2013); this lack of flexibility reduces the dissipation of energy and increases the degradation of ballast. Conversely, resilient rubber components such as under ballast mats (UBM) are commonly used to combat track degradation, noise, and vibration due to their damping properties (Kraskiewicz et al., 2021; Lima et al., 2017; Navaratnarajah & Indraratna, 2017; Sol-Sánchez et al., 2015).

End-of-life rubber conveyor belts discarded mostly from mining sites and minerals processing plants constitute a large source of rubber waste posing safety and environmental risks (Leong et al., 2023; Nuzaimah et al., 2018). Disposal is not only costly and labor intensive, depositing these rubber belts in landfills also has detrimental environmental effects (Tiwari et al., 2014). However, the rubber used to manufacture these conveyor belts is more robust and durable compared to most other types of rubber sheets, because it has been engineered to transport heavy and sharp items (Qi et al., 2024), therefore, recycling this heavy-duty rubber is advantageous from both technical and circular economy viewpoints. While under ballast mats (UBM) contribute to enhanced resilience to the overall track and assist in controlling the stress distribution with depth, they do not proactively limit the lateral displacement of ballast. In this respect, it seems imperative to create rubber grids (i.e. apertures cut on sheets) as a hybrid solution, whereby these rubber grids combine the resilience of UBMs with the particle interlocking provided by standard (polymer) geogrids. These grids also act as energy retention media during train passage, returning to their original shape upon unloading, thus releasing a portion of this stored strain energy, hence the description, Recycled Rubber Energy Absorbing Grid (REAG). Unlike a conventional UBM that absorbs energy mainly by compression in the vertical direction, REAG dissipates energy mainly through stretching in the transverse direction during dynamic loading by a moving train. The alternating stretching and relaxing of the rubber ribs struts during the cyclic loading-unloading (hysteretic) process leads to the absorption and dissipation of the energy, the rate and extent of which would depend on the viscoelastic properties of REAG. In essence, the process of energy dissipation of REAG under cyclic train loading enhances the overall energy capacity of the track system, thereby reducing the amount of energy transmitted to the ballast and thereby reducing both deformation and degradation of ballast while improving the structural performance of the track and its longevity.

In this study, large-scale process simulation tests were carried out at the University of Technology Sydney (UTS) to investigate the load-deformation response and degradation of ballast reinforced with REAG. The results from these large-scale tests, carried out with and without rubber grids, were analyzed with respect to the benefits of REAG on ballast performance. Additionally, this paper reports on the outcomes of field tests carried out at the Chullora Rail Precinct in NSW, Australia, to validate the feasibility and to evaluate the real-world applications of this innovative and sustainable solution. This environmentally friendly approach not only minimizes waste but also boosts the efficiency and durability of rail infrastructure, representing a significant advancement towards a greener and more resilient transportation network.

Large-Scale Laboratory Testing

Test Materials

The materials utilized in this study include fresh ballast, rubber grids (REAG), conventional capping material, and subgrade. The fresh ballast sourced from Albion Park Quarry in NSW, is made of latite basalt, a dense, fine-grained volcanic rock with sharply angular corners from blasting and quarrying. The physical properties of these basalt aggregates, which were assessed in accordance with the Australian Standards (AS 2758.7, 2015), signify that their high strength and angularity make them well-suited for railway ballast. This ballast sourced from the quarry was washed to eliminate any clay and dust, dried, sieved through specific mesh sizes, and combined in the correct proportions to attain the desired particle size distribution (PSD), as shown in Fig. 1. Particle size characteristics of ballast and capping material are presented in Table 1.

The rubber grids have been made using recycled conveyor belt rubber which has high strength and durability, and this heavy-duty material had been manufactured to withstand continual movement and tension, substantial attrition by heavy and angular particles (e.g. metal ore) and high temperature. These recycled rubber panels from the mining industry [Fig. 2(a)] were precisely cut with waterjet technology to form grids, at the UTS-TechLab [Fig. 2(b)]. This technology consists of an abrasive waterjet cutter with a linear accuracy of ±0.076 mm and a ball bar circularity of ±0.127 mm. The mechanical characteristics of the rubber material are detailed in Table 2. The rubber panels ranged from 10-11 mm thick, so the rubber grids were much thicker than standard polymeric geogrids. This increased thickness potentially enhances three-dimensional reinforcement, which, according to Makkar et al. (2019), would improve its performance under the high longitudinal stresses encountered in road and railway applications. These rubber grids [Fig. 2(c)] have 51 mm square apertures, a size determined by a prior study (Siddiqui et al., 2023), which found that this dimension was the most effective at mitigating impact forces.

The primary expense of REAG fabrication was the transportation of 10 rubber sheets, each measuring 1m × 1m, from the Pilbara metal mines in Western Australia to Sydney, which cost approximately AUD $1200. In contrast, cutting the apertures using a small waterjet cutter at the UTS engineering workshop, including the associated technical staff time, incurred a cost of less than AUD $400. Consequently, the total cost for producing the rubber grids amounted to less than AUD $16 per square meter. Once this novel application is commercialized, the cost of producing rubber geogrids from recycled conveyor belts is expected to become cost-competitive with conventional polymer-based geogrids.

Process Simulation Testing Apparatus

Cyclic-loading tests were carried out using the large-scale process simulation testing apparatus (PSTA) recently commissioned at the UTS. This prototype was designed to reproduce the influence zone or unit cell area of a standard heavy-haul track in Australia, to include a true triaxial chamber that can apply three principal stresses orthogonally, and also have four independent and movable vertical walls to mimic the lateral movement of ballast in an actual track, as shown in Fig. 3(a). The influence zone spans 400 mm on each side of a rail (800 mm total), which is one-third of the 2400 mm standard length of a concrete sleeper L (i.e., effective length, L_e= L/3 according to Jeffs and Tew (1991)) and extends 600 mm in the direction of train movement, thus matching the sleeper spacing (S_s). Unlike traditional geotechnical equipment with fixed boundaries, the PSTA has movable sides which prevent reduced scale effects and adverse boundary conditions, albeit its side boundary conditions may differ slightly from field conditions. A standard concrete sleeper (220 mm in width and 200 mm in height) was prepared to a length of 780 mm to fit inside the testing chamber. The 1 m deep test chamber can contain the typical 250-300 mm depth of ballast used in tracks and the layers beneath it. A plane strain condition was achieved by minimizing lateral strain in the longitudinal direction (perpendicular to the sleeper), simulating a long straight section of track (i.e., ε_2=0). The side walls parallel to the longitudinal direction were adjusted to maintain an applied confining pressure at 15 kPa, thus simulating the typical lateral confinement range of 10-30 kPa observed in Australian tracks as measured in the field by Indraratna et al. (2011).

Each vertical wall can move independently by up to 50 mm from its starting position; their movement, and horizontal stress are regulated by hydraulic jacks connected to load cells and by Linear Variable Differential Transformers (LVDTs). The walls were equipped with hinges and both linear and roller bearings to enable lateral movement with minimal friction. The applied cyclic stress and frequency were controlled by a servo-hydraulic actuator connected to a 100 kN load cell. A control system attached to a host computer and the accompanying manufacturer-inbuilt software were used to monitor and record the wall movements, the applied loads, and the readings from pressure cells and strain gauges [Fig. 3(b)]. Figure 3(c) shows a complete ballast specimen prepared for the test.

Test Procedure, Instrumentation and Loading

A 350 mm thick layer of subgrade was compacted at the bottom of the testing box to achieve a field density of 1730 kg/m^3 [Fig. 4(a)], and then a 150 mm thick capping layer was placed and compacted to achieve a field density of 2100 kg/m^3 [Fig. 4(b)]. For tests including REAG, a layer of REAG was placed above the capping layer separated by a woven fabric [Fig. 4(c)]. The ballast layer was then placed and compacted into three 100 mm thick layers (top, middle, and bottom); each layer was compacted to a standard field density of 1560 kg/m^3, using a vibratory compactor. A rail-sleeper setup was then placed on top of and in the center of the ballast layer. The spaces surrounding the sleeper were then filled with a 150 mm thick layer of crib ballast [Fig. 4(d)]. After testing, the ballast directly beneath the sleeper was recovered for breakage analysis. The three 100 mm thick layers of ballast particles under the sleeper (top, middle and bottom) were sprayed with water-based acrylic paint for easy identification [Figs. 4(e and f)], noting that the paint has minimal impact on particle friction (Navaratnarajah & Indraratna, 2017; Sweta & Hussaini, 2018).

The laboratory setup included load cells, LVDTs, pressure cells, strain gauges, and settlement pegs. The vertical and lateral loads were monitored by load cells connected to the main actuator and the side walls, respectively. Lateral deformation was monitored via LVDTs connected to the vertical walls and the external frame. Granular soil-type pressure cells (230 mm in diameter, 25 mm thick, capacity of 1 MPa) were strategically placed at the interfaces to measure vertical stresses at the sleeper-ballast interface, the ballast-capping interface, the capping-subgrade interface, and at a depth of 250 mm under the capping-subgrade interface [Fig. 4]. The vertical deformation of ballast was measured using settlement pegs placed at the sleeper-ballast and ballast-capping interfaces. The initial readings of these instruments were recorded before the cyclic loading tests commenced, and then continuous data was collected by data loggers at specified intervals (e.g., 20, 50, 100, 500, 1,000, 5,000, 10,000, 50,000, 100,000, 150,000, 200,000 and 250,000 cycles). The readings from the settlement pegs were taken manually at given load cycles.

The PSTA setup was used to replicate the typical cyclic loading endured by rail tracks. This involved using a servo-hydraulic actuator to apply the load through a 100 mm diameter cylindrical steel ram, which then transmits it onto the ballast via a rail-concrete sleeper setup [Fig. 3(a)]. The load application began with a stress-controlled loading that increased at 0.05 kN/s until it reached the minimum cyclic stress level of $\sigma_{1cyc,min}$= 30 kPa, which corresponds to the unloaded track weight (Navaratnarajah et al., 2018). After that, the cyclic loading commenced with a harmonic sinusoidal pattern using the dynamic actuator. The loading amplitude (A) and maximum cyclic stress ($\sigma_{1cyc,max}$) were determined based on simulated axle loads of 25 and 42 tonnes. The 25-tonne load represents typical coal freight trains (Indraratna et al., 2010), while the 42-tonne load represents the iron ore freight trains typically found at Pilbara, Western Australia. Atalar (2001) found that 30-60% of the wheel load is carried by the sleeper directly beneath it, with the remainder distributed to adjacent sleepers. It was assumed in this study that 40% of the wheel load goes to the sleeper directly below and 60% to adjacent sleepers. Therefore, with a 25-tonne axle load, the rail seat load (q_r) was 49.1 kN (q_r = 0.4×

(25/2) × 9.807 = 49.1 kN). The maximum stresses ($\sigma_{1cyc,max}$) were calculated using the AREA (American Railway Engineering) method (Li & Selig, 1998) as given below (Eq. 1):

$$\sigma_{1cyc,max} = \left(\frac{q_r}{BL_e}\right) F \tag{1}$$

where, B represents the width and L_e denotes the effective length of the sleeper. q_r is the rail seat load and F is a factor that varies based on the type of sleeper and track maintenance. Assuming a newly constructed track (F=1) with L_e = 0.8, B = 0.26 mm, the maximum stress ($\sigma_{1cyc,max}$) for a 25-tonne axle load would be 236 kPa, and for a 42-tonne axle load, $\sigma_{1cyc,max}$ comes to 396 kPa. These stresses are consistent with the field observations recorded by Indraratna et al. (2010). For the tests simulating a 25-tonne axle load, frequencies of 15 Hz, 20 Hz, and 25 Hz were used to represent train speeds of 110 km/h, 145 km/h and 182 km/h respectively, whereas the tests for the 42-tonne axle load were carried out at frequencies of 10 Hz, 15 Hz, and 20 Hz to represent train speeds of 72 km/h, 110 km/h and 145 km/h, respectively. A total of 250,000 load cycles were applied in each test. Twelve tests were performed in total. Table 3 provides an overview of the laboratory experiment program conducted in this study.

Results and Discussion

Measured Lateral and Vertical Deformation of Ballast

Figure 5 shows the lateral, vertical deformation and the volumetric strain of ballast with and without REAG, measured at different loading frequencies under axle loads of 25 and 42 tonnes. It was observed that the lateral displacement of ballast significantly reduces with the inclusion of REAG [Fig. 5(a)]. Table 4 presents the reduction in lateral displacement under varying axle loads and loading frequencies. This substantial reduction can be attributed to effective particles interlocking within the REAG apertures, which restricts their movement. The stabilization of lateral displacement after 10,000 cycles indicates that the interlocking of ballast with REAG remains consistent even with increased loading cycles. An increase in the loading frequency resulted in increased lateral displacements as expected, indicating that an increase in train speed increases the lateral displacement. Compared to traditional polymer geogrids (Hussaini et al., 2015), and under ballast mats (Navaratnarajah & Indraratna, 2017) the REAG was more effective in minimizing lateral displacement. This was due to the enhanced reinforcement and better interlocking provided by the three-dimensional apertures of REAG.

The vertical deformation (settlement) in Fig. 5(b) shows within the first 10,000 cycles there is a rapid increase for both types of tests, but as further load cycles are applied, the rate of settlement decreases, which corroborates with the reduced rate of lateral displacement towards attaining stable deformations. The rapid deformation of ballast during the first 10,000 load cycles is attributed to the initial densification in the early loading stages (particle rearrangement and re-compaction). It was observed that the vertical deformation of ballast significantly reduces with the inclusion of REAG. Table 4 presents the reduction in vertical deformation under varying axle loads and loading frequencies. The vertical deformation values for both the 25 and 42-tonne axle loads are below the 50 mm threshold specified in Australian and AREMA standards for rail tracks (AS 7635, 2013; AREMA, 2007). Furthermore, REAG has proven to be more effective than conventional polymer geogrids and under ballast mats at reducing settlement.

In the context of plane strain test conditions (i.e., $\varepsilon_2 = 0$), the volumetric strains (ε_v) were calculated using the equation below (Eq. 2).

$$\varepsilon_v = \varepsilon_1 + \varepsilon_3 \qquad (2)$$

where ε_1 represents the vertical strain and ε_3 denotes the lateral strain measured perpendicular to the rail direction.

Figure 5(c) shows the ε_v variations for axle loads of 25 and 42 tonnes. The contractive volumetric strain rises quickly and peaks around 10,000 cycles. The rate of increase then diminishes, eventually stabilizing at approximately 50,000 cycles. This data shows that with REAG, the volumetric strain of ballast decreases significantly for both 25-tonne and 42-tonne axle loads. These reductions are a further testament to ballast particles being trapped within the REAG apertures, unable to be freely displaced and rotated; this in turn results in reduced vertical and lateral deformation.

Strains in REAG

Two uniaxial strain gauges were attached to REAG in two orthogonal directions [Figure 6(a)] to measure the strains mobilized during the test. As shown in Fig. 6(b), the transverse tensile strains in REAG (parallel to the sleeper) are much greater than the longitudinal tensile strains perpendicular to the sleeper. The strains mobilized in REAG are summarized in Table 4. The minimal strains mobilized longitudinally are attributed to the plane strain condition simulating a long straight track. Observations indicated that the average tensile strain in the transverse direction increased with higher axle loads and loading frequencies, but it remained relatively unchanged longitudinally.

Ballast Breakage

In this study, the Ballast Breakage Index (BBI) developed by Indraratna et al. (2005) was adopted to calculate particle breakage. This method involves analyzing the PSD before and after testing in relation to a predetermined limit for maximum breakage, as shown in Fig. 7(a). Figure 7(b) shows examples of ballast breakage, including particle splitting and corner breakage. According to this approach the BBI is defined as (Eq. 3):

$$BBI = \frac{A}{A+B} \tag{3}$$

where, A indicates the shift in the PSD curve after testing and B signifies the area of potential breakage.

Ballast aggregates were recovered after each test and their particle size distribution (PSD) was analyzed to determine the BBI. The BBI values measured for tests subjected to axle loads of 25 and 42 tonnes and loading frequencies ranging from 10 to 25 Hz, with and without the inclusion of REAG, are shown in Fig. 7. It can be observed that there is a significant reduction in ballast breakage when the REAG is positioned at the ballast-capping interface. In fact, with REAG, the BBI in the top layer decreases by 18-21% for a 25-tonne axle load, while breakage in the middle and bottom layers decreases by 39-51% under the same loading conditions. For a 42-tonne axle load, breakage in the top layer decreases by 39-44% and by 28-54% in the middle and bottom layers. The larger reduction in BBI at the bottom layers may be attributed to ballast particles being in contact with the REAG layer, and thus decreasing a larger amount of energy. Moreover, REAG exhibit superior performance compared to conventional polymer geogrids in mitigating ballast breakage. A previous study carried out by Hussaini et al. (2015) under a 25-tonne axle load and 20 Hz loading frequency showed that the inclusion of a polymer geogrid only decreased the average BBI of about 10-33% after 250,000 load cycles. The enhanced ability of REAG to limit particle movement through increased confinement and to provide damping to the track substructure, reduces the energy absorbed by the ballast which in turn reduces particle breakage. For example, the damping ratios for high-density polyethylene, polyethylene, and polypropylene, which are used to create conventional polymer geogrids, range from 0.13-0.20, 0.01-0.07, and 0.05-0.07, respectively (Çolakoğlu, 2006; Rahman & Xu, 2023; Wang et al., 2019). In contrast, the damping ratio of the REAG material is 0.35, indicating improved performance in these applications. The energy observed by REAG will be described in the following sections.

Influence of Loading Frequency and REAG

Figures 8(a) and 8(b) show the effect of loading frequency on REAG in terms of lateral displacement and vertical deformation. It is evident that the lateral displacement and vertical deformation increase as the loading frequency and axle load increase. However, the inclusion of REAG significantly decreases ballast deformation. The effect of REAG can be summarized in term of the reduction factors related to lateral deformation, vertical deformation, and ballast breakage (R_f and $R_{f,breakage}$). They can be determined as (Eq. 4 and 5):

$$R_f = \frac{\delta_{unreinforced} - \delta_{reinforced}}{\delta_{unreinforced}} \times 100\% \tag{4}$$

$$R_{f,breakage} = \frac{BBI_{unreinforced} - BBI_{reinforced}}{BBI_{unreinforced}} \times 100\% \tag{5}$$

where, δ is the displacement in lateral or vertical direction.

Figure 8(c) shows that the lateral displacement reduction factor ($R_{f,lateral}$) for the 25-tonne and 42-tonne axle loads decrease as the loading frequency increases and its value ranges from 40%-55%. Conversely, the reduction factor for settlement ($R_{f,vertical}$) remains higher, varying slightly with frequencies between 52-61% for both axle loads. With the 25-tonne axle load, the ballast breakage reduction factor ($R_{f,breakage}$) decreases from 38% to 36.5% when the loading frequency rises from 15 Hz to 25 Hz, whereas in the 42-tonne axle load tests the breakage reduction factor increases from 39% to 45% as the loading frequency increases from 10 Hz to 20 Hz. This implies that REAG provides greater benefits when placed in heavy-haul (freight) lines rather than the lighter passenger train lines.

Resilient Modulus.

The resilient modulus (M_R) is a key parameter in designing track foundations subjected to cyclic loads (Naeini et al., 2019). Figure 9(a) shows the typical stress-strain hysteresis loop of a prototype track obtained from the cyclic loading test of the simulated track element. In this study, the resilient modulus of the entire layered substructure assembly was assessed, hence called the resilient track modulus (M_{RT}). The transient stress-strain data measured at the selected number of loading cycles (N) were utilized to determine the resilient track modulus (M_{RT}), energy dissipation (E_d) and the damping ratio (D), as shown in Fig. 9(b). M_{RT} is defined as (Eq. 6):

$$M_{RT} = \frac{\Delta\sigma_{1cyc}}{\varepsilon_r} \tag{6}$$

where, $\Delta\sigma_{1cyc} = \Delta\sigma_{1cyc,max} - \Delta\sigma_{1cyc,min}$ and ε_r is elastic strain recovered during unloading.

The variations of M_{RT} with the loading cycles for different tests are shown in Fig. 10. As anticipated, the resilient track modulus (M_{RT}) increases with an increase in N up to 100,000 load cycles and then gradually reaches a plateau. This increase in M_{RT} in the initial loading stage is partially due to the cyclic compaction of ballast as the compressive volumetric strain (ε_v) increases with N to create a reduced void ratio. Figure 10 also shows that an increase in the load from 25 tonnes [Fig. 10(a)] to 42 tonnes [Fig. 10(b)], and the loading frequency (from

10 to 25 Hz) leads to a higher compaction of particles which contributes to a further increase in M_{RT}. Furthermore, higher frequencies help smaller particles relocate into the voids between larger particles, enhancing ballast densification while increasing the magnitude of M_{RT}. The test results showed that the inclusion of REAG leads to a 5–15% increase in the M_{RT} indicating elastic (recoverable) strain during cyclic loading decreases with REAG.

Based on test data, an empirical expression is introduced to predict the resilient track modulus by capturing the effect of the loading frequency, the size of REAG apertures, and the number of loading cycles, as given by Eq. 7.

$$M_{RT} = \left[\frac{f^2}{1-\alpha A_R}(K_1 + K_2 logN)\right]^n \quad (7)$$

where, f = loading frequency (Hz), A_R = aperture size of REAG (m), and N = number of load cycles.

The value of α is set to 0 when REAG is absent and 1 when REAG is present. Additionally, n = 2/3 and k_1 and k_2 are the regression model parameters. It is seen from Fig. 10 that the M_{RT} values predicted by the empirical model with and without the inclusion of REAG, match those measured from the tests for 25 and 42-tonne axle loads quite well (R^2>0.95).

Energy Dissipation and Damping Ratio of the Track

During cyclic loading and unloading, ballast exhibits hysteresis behavior, which dissipates the mechanical strain energy. This energy absorption and dissipation mechanism is related to the mechanical damping characteristics of viscoelastic materials. Energy dissipation is linked to the area within the hysteresis loop [Fig. 9(b)] and represents the energy dissipation per unit volume for each loading and unloading cycle. The damping ratio indicates the fraction of energy dissipated compared to the energy stored during the loading and unloading cycle (Sitharam & Vinod, 2010). The energy dissipation per cycle (E_d) and damping ratio (D) are defined by the following fundamental algebraic expressions (Eq. 8 and 9):

$$E_d = A_L \tag{8}$$

$$D = \frac{A_L}{4\pi A_S} \tag{9}$$

where, A_L = area of the hysteresis loop, and A_S = area of the shaded right triangle.

At specific load cycle intervals, at least 5 consecutive hysteresis loops were used to calculate D and E_d, with the average of these 5 values being taken for further analysis. Figure 11 shows the variation of D and E_d with N for axle loads of 25 and 42 tonnes, respectively. It is observed that REAG increases the damping ratio (D) of the track substructure, resulting in greater strain energy dissipation. Based on Fig. 11, D and E_d are both elevated and then decrease with N. The elevated energy dissipation in the initial load cycles is due to the significant loss of energy from plastic sliding and particle breakage. The damping ratio and energy dissipation per cycle stabilize when the ballast mass densifies and stabilizes the deformation after about 20,000 cycles. This increased dissipation happens through particle sliding and breakage and is directly proportional to the added input energy. The previous study conducted by Navaratnarajah and Indraratna (2017) under 25-tonne axle load showed that the inclusion of UBMs enhances the dissipation of track energy by 36-95%, whereas REAG only increases it by 25-51%. This comparative reduction in energy dissipation by REAG occurred because the volume of rubber incorporated into the track was less than the UBMs.

Based on test data (Fig. 11), an empirical formula can be derived to calculate the total energy dissipation (E_D) per unit volume across the entire track structure, incorporating the energy dissipated through the frictional sliding of ballast (E_S), ballast breakage (E_B), the rubber grid (E_R), and other substructure layers (E_{SC}) as follows (Eq. 10):

$$E_D = E_S + E_B + E_{SC} + (1-\alpha)E_R \tag{10}$$

where, the value of α is set to 1 when REAG is absent and 0 when REAG is present.

It is noted that E_S correlates directly with the applied cyclic stress ($\Delta\sigma_{cyc}$) and the total shear strain (ε_S), with more energy needed to surpass the shear resistance from inter-particle friction (Liu et al., 2014). E_S can be determined by (Eq. 11):

$$E_S = a\left(\Delta\sigma_{cyc}\varepsilon_s\right) \tag{11}$$

E_B depends on the breakage of ballast, and can be estimated using the equation (Eq. 12) proposed by Navaratnarajah and Indraratna (2017):

$$E_B = b(k \times BBI)^c \tag{12}$$

where, k = the axle load factor adjusted based on a minimum axle load P_m. $k = \sqrt{P/P_m}$ where P is the simulated axle load, P_m =20 tonnes for the Australian standard heavy haul, and a, b, and c are empirical model parameters.

The energy dissipated in the subgrade layer is highly influenced by the density of the soil (Wang & Yan, 2012). Moreover, the vertical stress gradient within the soil impacts its vibration and subsequent energy dissipation (Luan et al., 2019; Zheng et al., 2022), as areas with greater stress gradients are likely to undergo larger shear strains and more significant energy dissipation. Consequently, an equation (Eq. 13) is proposed herein to calculate E_{SC}:

$$E_{SC} = d(\rho_{SC} \times \nabla\sigma_{SC}^{2})^{e} \tag{13}$$

where, d and e are empirical model parameters, $\nabla\sigma_{SC}$ = vertical stress gradient within the capping and subgrade layers, and ρ_{SC} = equivalent density of compacted capping and subgrade layers (kg/m^3), as given (Eq. 14):

$$\rho_{SC} = \frac{\rho_c h_c + \rho_{sg} h_{sg}}{h_c + h_{sg}} \tag{14}$$

where, ρ_C and ρ_{sg} are the compacted densities of the capping and subgrade material respectively, and h_C and h_{sg} are the thicknesses of the capping and subgrade layers in the test specimen respectively.

To calculate the energy dissipated by the REAG (E_R), the material properties, the geometry of REAG, and the mobilized strains, as shown in Figure 6b, must be considered. The mobilized strains are almost proportional to the vertical stress at the ballast-capping interface, hence the following empirical equation (Eq. 15) can be introduced to predict the E_R:

$$E_R = \frac{G"}{4}\left(t \times K_{A,eff}^{f} \times \sigma_{BC}^{g}\right) \tag{15}$$

where, G'' = viscoelastic loss modulus of rubber (Pa/m), t = thickness of the REAG (m), $K_{A,eff}$ = effective area ratio of the REAG determined by Siddiqui et al. (2023), σ_{BC} = maximum vertical stress at the ballast capping interface (kPa), and f and g are empirical model parameters.

The magnitude of G'' can be calculated from Ferry (1980), where the rubber material was modeled using the generalized Maxwell theory as given by (Eq. 16):

$$G'' = \sum_{i=1}^{n} \frac{G_i \omega \tau_i}{1+\omega^2 \tau_i^2} \quad (16)$$

where, G_i = spring constant of ith Maxwell element (Pa/m), τ_i = relaxation time of ith Maxwell element (s), and ω = loading frequency (Hz). G_i and τ_i are also called viscoelastic prony series parameters whose values are obtained from Mayuranga et al. (2022), and n represents the number of Maxwell elements (Fliigge, 1967; Roylance, 2001).

Based on the above model, a nonlinear regression analysis is carried out to predict the total energy dissipation (E_D) of the test specimen. Figure 12 shows a comparison between the predicted E_D values and those derived from the test data. It is observed that the predicted values of E_D corroborate well with the measured laboratory test data ($R^2 > 0.97$).

Measured Stress Distribution with Depth

Figure 13 shows the distribution of vertical stress with depth under axle loads of 25 and 42 tonnes at varying frequencies. Pressure cells installed at different interfaces within the layered track substructure setup recorded these stresses. As expected, the test results show that the stresses within the substructure layers increase with the axle load and the loading frequency, and align closely with the data obtained from field observations and laboratory tests (Indraratna et al., 2021; Indraratna et al., 2014; Navaratnarajah & Indraratna, 2017). It was found that placing a layer of REAG at the ballast-capping interface significantly reduces the stresses in the track substructure. Table 5 presents the average reduction of vertical stress at different locations in the track substructure. It is also noted that placing a rubber grid beneath the ballast layer did not significantly alleviate stress at the sleeper-ballast interface. Other studies have indicated that attaching a rubber pad directly under sleeper proved to be effective in reducing stress at the sleeper-ballast interface (Abadi et al., 2015; Navaratnarajah & Indraratna, 2017).

The largest reduction in stress occurs at the ballast-capping interface where REAG was positioned. The most substantial reduction in stress was observed at the ballast-capping interface where the REAG was positioned. This can be attributed to the damping properties of the rubber material, thus leading to a reduction in the stresses transmitted to the underlying substructure layers.

As discussed above, laboratory test results show that the REAG significantly enhances the performance of ballast tracks under cyclic loading. However, it is crucial to predict its performance in the field, where actual moving train loading with different wheel loads and boundary effects are present. While tests using the PSTA are valuable for demonstrating the concept, more reliable results can be obtained through field testing, where the subgrade depth is unlimited. In laboratory tests, even with a subgrade layer included, the presence of a fixed boundary at the bottom of the 350 mm subgrade limits the replication of real-world conditions. This artificial boundary alters stress propagation, leading to discrepancies compared to field conditions where the subgrade is unrestricted. Having demonstrated the concept and effectiveness of REAG in large-scale laboratory testing, at the request of Sydney Trains a field test was carried out on a fully instrumented track in Chullora (suburb of Western Sydney), with the objective of adopting REAG for real-life applications. This is discussed in detail in the following section.

Field Testing

Construction of REAG Section

The section of test track built at the Chullora Technology Precinct, NSW, Australia has a 20 m long REAG section over a 100 m long instrumented track as a control. The substructure consists of a compacted fill layer [Fig. 14(a)], followed by a thin layer of sandy clayey silt, underlying silty clays, and a bedrock of stiff clay interspersed occasionally with shale. Site investigation was conducted to establish the geological profile for shallow depth below the track site (up to 5m) with the relevant soil parameters used in the track design. Based on Atterberg limits, the plastic and liquid limits were 24% and 36% respectively, where the natural water content was 18%. The soil could be categorized as clayey silt of low plasticity (CL-ML) in the USCS soil classification.

For the entire track, fresh ballast of nominal 60-graded specification (AS 2758.7, 2015) was used. The maximum dry densities of the ballast and capping layers are presented in Table 3. In the REAG section, rubber grids made of end-of-life conveyor belts had exactly the same geometric characteristics and engineering properties as those tested in the laboratory. These grids were placed at the interface between the capping and ballast layers [Fig 14(e)]. Both the control and REAG sections were constructed with a 250 mm thick layer of ballast and a 200 mm thick capping layer, following the technical standards for heavy-haul (Transport for NSW, 2018).

Both sections utilized the same track components, including precast concrete sleepers and AS60SC steel rails [Fig. 14(h)]. After removing 500 mm of the stiff clayey subgrade, a 200 mm thick granular drainage layer was placed on top of the clay surface to enhance drainage. A non-woven geotextile layer was also placed as a separator between the capping and ballast layers to prevent the ballast from being contaminated with fines segregated from the capping layer [Fig. 14(b)]. Figure 14 shows the phases of track construction during the field test.

Instrumentation and Train Loading Application

The vertical stresses in each track section were measured using 200 mm diameter pressure cells installed horizontally between the sleeper and the ballast, the ballast and the capping layer [Fig.

14(d)], and between the capping layer and the subgrade. Settlement pegs were placed at the same interfaces to monitor the settlement [Fig. 14(d)], and triaxial accelerometers were attached to the sleepers in both the standard and rubber grid sections to measure the accelerations. Strain gauges were positioned at multiple points on the rubber grid to record the mobilized strains, as shown in Fig. 14(f).

Flexible conduits were used to protect the electrical connections to the sensors and prevent damage during track operations. These cables fed into a high-speed data acquisition system housed in cabinets beside the track. This system was powered by solar cells and batteries for increased independence. It was triggered automatically and collected data at a sampling rate of 50 Hz.

A diesel locomotive (22.5 tonne axle load) with two coal-filled wagons was utilized to travel back and forth along this trial track at a maximum speed of less than 20 km/h, to conform to the speed limit set by Sydney Trains for this location. During the testing phase the train completed a total of 1003 passes (6018 axle passes) along the track. The field test was conducted over 6 days, during which 168, 180, 180, 131, 204, and 140 train passes were applied daily (daytime) on consecutive days. On each testing day, the loading phase was 8 hours. The time duration between two train passes was approximately 72-96 seconds.

Results and Discussion

Vertical Stress Distribution

Figure 15 shows the changes in vertical stress across various interfaces (depths) of the track substructure during the 600th, 1296th, and 2544th axle passes in the standard and REAG sections. Compared to the standard track, the REAG section showed a decrease in stress at the sleeper-ballast interface of 21%, 7%, and 16% for the 600th, 1296th, and 2544th axle passes, respectively, while the respective reductions in stress at the ballast-capping interface were 14%, 11%, and 27%. These measurements are in good agreement with those measured from the large-scale cubical tests, where the stress reductions at the sleeper-ballast and ballast-capping interfaces for 25-tonne axle load were 4.2% and 21.6%, respectively. However, there was no significant change in vertical stress at the subgrade-capping interface, indicating that while REAG was effective in reducing stress in the ballast and capping layers, it had less influence on the underlying subgrade. Despite minor variations in the subgrade soil conditions between sections, the vertical pressure at the top of the subgrade was consistent in the proximity of 40 kPa. This suggests minimal deformation of the subgrade layer due to its composition of relatively dry and compacted sandy/silty clay about 2 - 3 m deep, underlain by bedrock consisting primarily of shale interspersed with claystone.

Track Settlement

Settlement pegs were surveyed before the train loading to set baseline values. Survey measurements were taken daily throughout the loading phase to monitor changes in elevation. Figure 16 shows the cumulative settlement for both the standard and REAG sections of track, plotted against the number of train passes. The field measurements show that track sections experienced significant settlement during the first 2400 axle passes, beyond which it reached a plateau. For instance, the standard track exhibits a settlement of 9.3 mm while the REAG track shows a settlement of about 7.6 mm. Notably, after 1003 train passes the sections with the rubber grid exhibited about 18.3% less settlement. This reduced settlement can be attributed to REAG enhancing ballast confinement through particle interlocking and energy dissipation, as demonstrated by large-scale testing that indicated a significant increase in energy dissipation corresponding to the increased damping ratio of the track element.

Measured Acceleration

Figure 17 shows a comparison of the acceleration from both instrumented sections of track at different stages of train loading, as measured by accelerometers positioned on top of the sleeper. The set of data shows that compared to a standard track, the inclusion of REAG significantly decreases the peak acceleration (i.e., track vibrations) by 54%, 74%, 63%, and 63% at 600, 3000, 4800, and 6000 axle passes respectively.

It is noteworthy that the relatively low acceleration observed in this field test is attributed to the low train speed of 15-20 km/h applied during testing. These figures are consistent with the findings by Baldonedo et al. (2019), which link the track acceleration to the train speed. Despite these low speeds, the ability of rubber grid to reduce vibrations is evident, which is particularly promising given the increasing concerns about track vibration and noise, especially in urban settings.

Mobilized Strains in REAG

The longitudinal strain (along the rail) and transverse strain (parallel to the sleepers) mobilized in the REAG during the passage of trains are plotted in Fig. 18. It shows that the maximum tensile strain mobilized in the transverse direction is about 750 μ/m, while in the longitudinal direction the maximum compressive strain is around 370 μ/m. These values equate to strains of about 0.75% and 0.37%, respectively. These mobilized strains within the rubber grid are likely due to the interlocking effect between the grid and the surrounding ballast aggregates. The higher tensile strains in the transverse direction are due to the additional confinement provided by REAG, which in turn decreases the lateral displacement of ballast, as also observed in the cubical process simulation testing. The comparatively small compressive strains in the longitudinal direction support the plane strain conditions. Moreover, the minimal compressive strains mobilized within REAG in the vertical direction indicate that the compression of REAG is insignificant in the overall track settlement.

Conclusions

This study assessed the performance of ballasted tracks enhanced with REAG by conducting extensive laboratory tests involving cyclic loading at various frequencies and axle weights, and fully operational field trials in Chullora (suburb of Western Sydney). Based on these laboratory and field tests, the following conclusions can be drawn:

- Placing rubber grids under the ballast layer resulted in an estimated 40-55% decrease in lateral displacement and about 50-60% decrease in settlement, compared to the traditional polymer geogrids and conventional under-ballast mats, which could only reduce lateral displacements by 16-21% and 8-9% respectively, and settlement by 49-58% and 9-22% respectively. These observations proved that REAG would be more effective in controlling the overall deformation of the ballast layer under cyclic loading in contrast to traditional geo-inclusions used in track substructure stabilization.
- The overall degradation (breakage) of ballast was reduced by about 20-55% with the introduction of REAG. The maximum reduction in breakage (40-55%) occurred at the bottom layer where the rubber grids reinforced the ballast and dampened the dynamic stress amplification. For instance, with 25-tonne axle load, the average breakage of ballast decreased from 8.54% to 5.63% at a loading frequency of 25 Hz. REAG was more effective than conventional polymer geogrids at reducing ballast breakage. For instance, under a 25-tonne axle load and 20 Hz loading frequency, the BBI reduction of polymer geogrid reinforced ballast was 10-33% after 250,000 load cycles, whereas the average BBI reduction of REAG reinforced ballast under similar conditions was 37%. These promising results lead to the conclusion that in practice, REAG would be able to extend track longevity and reduce the cost of track maintenance associated with ballast degradation.

- It was noted that REAG improved the damping characteristics of the track substructure. For instance, for a 25-tonne axle load, the damping ratio (D) of the track element increased by 14-32% with the inclusion of REAG. This improved damping led to a 25-51% increase in the dissipation of energy per cycle of the track element (E_d). In addition, REAG improved the resilient track modulus (M_{RT}) by 7.0-13.3%, thereby offering improved control of track deformation. These results prove beyond doubt that the rubber grids perform as effective damping elements to offer significant benefits in terms of reducing both track deformation and degradation.
- Installing a layer of REAG at the ballast-capping interface substantially lowered the stress levels beneath the track substructure. For example, with a 25-tonne axle load, the reductions were about 4.2% at the sleeper-ballast interface, 21.6% at the ballast-capping interface, 13.2% at the capping-subgrade interface, and 11.3% at 250 mm below the capping layer within the subgrade. For a 42-tonne axle load, the corresponding reductions were 3.2%, 11.9%, 9.3%, and 5.9%, respectively at similar interfaces. These findings clearly demonstrate that the rubber grids are highly effective in significantly reducing the stress levels in the track substructure layers.
- The field results also indicated that REAG when placed beneath the ballast layer could reduce the vertical stress by approximately 7-20% at the sleeper-ballast interface and 11-27% at the ballast-capping interface. After 6000 axle passes, the track settlement with REAG decreased by about 18.3%. Moreover, the placement of these rubber grids resulted in a 54-74% decrease in the vertical acceleration of the rail. In real life situations, this observation leads to the conclusion that the use of REAG is particularly advantageous for heavy-haul tracks built over soft subgrade deposits with high water content, which may otherwise experience premature yielding in the absence of effective control of the vertical stress distribution with depth.

Declarations

Data Availability Statement

Some or all data, models, or code that support the findings of this study are available from the corresponding author upon reasonable request.

Conflicts of Interest

The authors all declare no conflict of interest.

Acknowledgments

The authors gratefully acknowledge the financial support provided by the Australian Research Council through grants ARC LP200200915 and ARC DP220102862. They also express their gratitude for the financial and technical assistance from industry partners including Transport for NSW (formerly Sydney Trains) and Bridgestone Corporation. The authors are also thankful to the technical staff at UTS-TechLab (c/o Dr Hossein Haddad, Mr. Rami Haddad, Mr. Alex Withey, and Mr. Melvin Montecino) for their assistance during the experimental program.

References

Abadi, T., Le Pen, L., Zervos, A., & Powrie, W. (2015). Measuring the area and number of ballast particle contacts at sleeper/ballast and ballast/subgrade interfaces. *The International Journal of Railway Technology*, *4*(2), 45-72.

AREMA (2007). Manual for railway engineering, Chapter 5, (American Railway Engineering and Maintenance-of-Way Association). Lanham, MD.

Arulrajah, A., Abdullah, A., Bo, M. W., & Bouazza, A. (2009). Ground improvement techniques for railway embankments. Proceedings of the Institution of Civil Engineers-Ground Improvement, 162(1), 3-14.

AS 1333. (2019). Conveyor belting of elastomeric and steel cord construction (Reconfirmed 2019). In: Sydney, NSW, Australia: Standards Australia Limited.

AS 2758.7. (2015). Aggregates and rock for engineering purposes, Part 7. Railway ballast. In: Sydney, NSW, Australia: Standards Australia Limited.

AS 7635 (2013). Railway Infrastructure – Track Geometry. In: Sydney, NSW, Australia: Standards Australia Limited.

ASTM. (2018). D 575-91: Standard test methods for rubber properties in compression. In: West Conshohocken, PA, USA: ASTM International.

ASTM. (2021a). 412-16: Standard test methods for vulcanized rubber and thermoplastic elastomers – tension. In: West Conshohocken, PA, USA: ASTM International.

ASTM. (2021b). D 2240-15: Standard test method for rubber property – durometer hardness. In: West Conshohocken, PA, USA: ASTM International.

Atalar, C. (2001). Settlement of geogrid-reinforced railroad bed due to cyclic load. Proc. 15th Int. Conf. on Soil Mech. and Geothch. Engrg.,

Baldonedo, J., López-Campos, J. A., López, M., Casarejos, E., & Fernández, J. R. (2019). Optimization of the auxiliary-beam system in railway bridge vibration mitigation using FEM simulation and genetic algorithms. *Symmetry*, *11*(9), 1089.

Bathurst, R. J., & Raymond, G. P. (1987). Geogrid reinforcement of ballasted track. *Transp. Res. Rec*(1153), 8-14.

Chrismer, S., & Davis, D. (2000). Cost comparisons of remedial methods to correct track substructure instability. *Transportation research record*, *1713*(1), 10-14.

Çolakoğlu, M. (2006). Damping and vibration analysis of polyethylene fiber composite under varied temperature. *Turkish Journal of Engineering and Environmental Sciences*, *30*(6), 351-357.

Correia, A. G., Winter, M., & Puppala, A. (2016). A review of sustainable approaches in transport infrastructure geotechnics. Transportation Geotechnics, 7, 21-28.

Ferry, J. D. (1980). *Viscoelastic properties of polymers*. John Wiley & Sons.

Fliigge, W. (1967). Viscoelasticity. *Blaisdell Publ. Comp., London*, 1069-1084.

Gładysiewicz, L., Konieczna-Fuławka, M., & Woźniak, D. (2019). Determining of damping factor of belt on the basis of hysteresis loop in calculation of conveyor belt rolling resistance. *International Multidisciplinary Scientific GeoConference: SGEM*, *19*(1.3), 209-216.

Göbel, C. H., Weisemann, U. C., & Kirschner, R. A. (1994). Effectiveness of a reinforcing geogrid in a railway subbase under dynamic loads. *Geotextiles and Geomembranes*, *13*(2), 91-99. https://doi.org/https://doi.org/10.1016/0266-1144(94)90041-8

Hatami, K., Mahmood, T., Ghabchi, R., & Zaman, M. (2013). Influence of In-Isolation Properties of Geogrids on Their Pullout Performance in a Dense Graded Aggregate. *Indian Geotechnical Journal*, *43*(4), 303-320. https://doi.org/10.1007/s40098-013-0060-8

Horníček, L., Tyc, P., Lidmila, M., Krejčiříková, H., Jasanský, P., & Břeštovský, P. (2010). An investigation of the effect of under-ballast reinforcing geogrids in laboratory and operating conditions. *Proceedings of the Institution of Mechanical Engineers, Part F: Journal of Rail and Rapid Transit*, *224*(4), 269-277.

Hussaini, S. K. K., Indraratna, B., & Vinod, J. S. (2015). Performance assessment of geogrid-reinforced railroad ballast during cyclic loading. *Transportation Geotechnics*, *2*, 99-107. https://doi.org/10.1016/j.trgeo.2014.11.002

Indraratna, B., Arachchige, C. M. K., Rujikiatkamjorn, C., Heitor, A., & Qi, Y. (2024). Utilization of Granular Wastes in Transportation Infrastructure. *Geotechnical Testing Journal*, *47*(1). https://doi.org/10.1520/gtj20220233

Indraratna, B., Lackenby, J., & Christie, D. (2005). Effect of confining pressure on the degradation of ballast under cyclic loading. *Géotechnique*, *55*(4), 325-328.

Indraratna, B., Ngo, N. T., & Rujikiatkamjorn, C. (2013). Deformation of coal fouled ballast stabilized with geogrid under cyclic load. *Journal of Geotechnical and Geoenvironmental Engineering*, *139*(8), 1275-1289.

Indraratna, B., Ngo, T., Ferreira, F. B., Rujikiatkamjorn, C., & Tucho, A. (2021). Large-scale testing facility for heavy haul track. *Transportation Geotechnics*, *28*, 100517.

Indraratna, B., Nimbalkar, S., Christie, D., Rujikiatkamjorn, C., & Vinod, J. (2010). Field assessment of the performance of a ballasted rail track with and without geosynthetics. *Journal of Geotechnical and Geoenvironmental Engineering*, *136*(7), 907-917.

Indraratna, B., Nimbalkar, S., & Neville, T. (2014). Performance assessment of reinforced ballasted rail track. *Proceedings of the Institution of Civil Engineers. Ground improvement*, *167*(1), 24-34. https://doi.org/10.1680/grim.13.00018

Indraratna, B., Qi, Y., Ngo, T. N., Rujikiatkamjorn, C., Neville, T., Ferreira, F. B., & Shahkolahi, A. (2019). Use of Geogrids and Recycled Rubber in Railroad Infrastructure for Enhanced Performance. *Geosciences*, *9*(1), 30. https://doi.org/10.3390/geosciences9010030

Indraratna, B., Rujikiatkamjorn, C., & Salim, W. (2011). *Advanced rail geotechnology–ballasted track*. CRC press.

Jeffs, T., & Tew, G. (1991). A review of track design procedures-sleepers and ballast. *Railways of Australia, Vol 2, Australian Government Publishing Service, Melbourne, Australia.*

Kraskiewicz, C., Zbiciak, A., Wasilewski, K., & Al Sabouni-Zawadzka, A. (2021). Laboratory Tests and Analyses of the Level of Vibration Suppression of Prototype under Ballast Mats (UBM) in the Ballasted Track Systems. *Materials*, *14*(2), 313. https://doi.org/10.3390/ma14020313

Leong, S.-Y., Lee, S.-Y., Koh, T.-Y., & Ang, D. T.-C. (2023). 4R of rubber waste management: current and outlook. *Journal of material cycles and waste management*, *25*(1), 37-51.

Li, D., & Selig, E. T. (1998). Method for railroad track foundation design. I: Development. *Journal of Geotechnical and Geoenvironmental Engineering*, *124*(4), 316-322.

Lima, A. d. O., Dersch, M., Qian, Y., Tutumluer, E., & Edwards, J. (2017). Laboratory evaluation of under-ballast mat effectiveness to mitigate differential movement problem in railway transition zones. Proceedings of the 10th international conference on the bearing capacity of roads, railways and airfields,

Liu, H., Zou, D., & Liu, J. (2014). Constitutive modeling of dense gravelly soils subjected to cyclic loading. *International Journal for Numerical and Analytical Methods in Geomechanics*, *38*(14), 1503-1518. https://doi.org/10.1002/nag.2269

Luan, L., Zheng, C., Kouretzis, G., Cao, G., & Zhou, H. (2019). Development of a three-dimensional soil model for the dynamic analysis of end-bearing pile groups subjected to vertical loads. *International Journal for Numerical and Analytical Methods in Geomechanics*, *43*(9), 1784-1793.

Makkar, F. M., Chandrakaran, S., & Sankar, N. (2019). Performance of 3-D geogrid-reinforced sand under direct shear mode. *International journal of geotechnical engineering*, *13*(3), 227-235. https://doi.org/10.1080/19386362.2017.1336297

Mayuranga, H., Navaratnarajah, S., Bandara, C., & Jayasinghe, J. (2022). Numerical Simulation of Energy-Absorbing Rubber Pads Using FEM and DEM Approaches—A

Comparative Study. 12th International Conference on Structural Engineering and Construction Management: Proceedings of the ICSECM 2021,

Naeini, M., Mohammadinia, A., Arulrajah, A., Horpibulsuk, S., & Leong, M. (2019). Stiffness and strength characteristics of demolition waste, glass and plastics in railway capping layers. Soils and Foundations, 59(6), 2238-2253.

Navaratnarajah, S. K., & Indraratna, B. (2017). Use of rubber mats to improve the deformation and degradation behavior of rail ballast under cyclic loading. *Journal of Geotechnical and Geoenvironmental Engineering*, *143*(6), 04017015.

Navaratnarajah, S. K., Indraratna, B., & Ngo, N. T. (2018). Influence of under sleeper pads on ballast behavior under cyclic loading: experimental and numerical studies. *Journal of Geotechnical and Geoenvironmental Engineering*, *144*(9), 04018068.

Nuzaimah, M., Sapuan, S., Nadlene, R., & Jawaid, M. (2018). Recycling of waste rubber as fillers: A review, *368, 0122016*. IOP Conference Series: Materials Science and Engineering,

Qi, Y., Indraratna, B., Ngo, T., Arachchige, C. M. K., & Hettiyahandi, S. (2024). Sustainable solutions for railway using recycled rubber. *Transportation Geotechnics*, *46*, 101256. https://doi.org/https://doi.org/10.1016/j.trgeo.2024.101256 (https://www.sciencedirect.com/science/article/pii/S2214391224000771)

Rahman, M. Z., & Xu, H. (2023). Damping under Varying Frequencies, Mechanical Properties, and Failure Modes of Flax/Polypropylene Composites. *Polymers*, *15*(4), 1042.

Roylance, D. (2001). Engineering viscoelasticity. *Department of Materials Science and Engineering–Massachusetts Institute of Technology, Cambridge MA*, *2139*, 1-37.

Selig, E. T., & Waters, J. M. (1994). *Track geotechnology and substructure management*. Thomas Telford.

Siddiqui, A., Indraratna, B., Ngo, T., & Rujikiatkamjorn, C. (2023). Laboratory assessment of rubber grid-reinforced ballast under impact testing. *Géotechnique Letters*, *13*(2), 1-11.

Sitharam, T., & Vinod, J. S. (2010). Evaluation of shear modulus and damping ratio of granular materials using discrete element approach. *Geotechnical and Geological Engineering*, *28*, 591-601.

Sol-Sánchez, M., Moreno-Navarro, F., & Rubio-Gámez, M. C. (2015). The use of elastic elements in railway tracks: A state of the art review. *Construction and Building Materials*, *75*, 293-305.

Sweta, K., & Hussaini, S. K. K. (2018). Effect of shearing rate on the behavior of geogrid-reinforced railroad ballast under direct shear conditions. *Geotextiles and Geomembranes*, *46*(3), 251-256.

Tiwari, B., Ajmera, B., Moubayed, S., Lemmon, A., Styler, K., & Martinez, J. G. (2014). Improving geotechnical behavior of clayey soils with shredded rubber tires—Preliminary study. Geo-Congress 2014: Geo-characterization and Modeling for Sustainability

Transport for NSW. (2018). T HR CI 12111 SP Earthwork Materials. In *T HR CI 12111 SP*

Wang, J., & Yan, H. (2012). DEM analysis of energy dissipation in crushable soils. *Soils and Foundations*, *52*(4), 644-657.

Wang, X., Yu, Z., & McDonald, A. G. (2019). Effect of different reinforcing fillers on properties, interfacial compatibility and weatherability of wood-plastic composites. *Journal of Bionic Engineering*, *16*, 337-353.

Zheng, C., Kouretzis, G., Ding, X., & Luan, L. (2022). Vertical vibration of end-bearing single piles in poroelastic soil considering three-dimensional soil and pile wave effects. *Computers and Geotechnics*, *146*, 104740.

List of Tables

Table 1. Particle size characteristics of fresh ballast and capping material (data from Indraratna et al., 2024)

Materials	d_{max} (mm)	d_{min} (mm)	d_{50} (mm)	C_u	C_c	Maximum dry density (t/m^3)
Ballast	63	9.5	37.5	2.84	1.42	1.6
Capping	19	0.044	2.36	75.4	1.2	2.2

Table 2. Mechanical characteristics of rubber material used in this study (Values obtained from Siddiqui et al., 2023)

Properties	Values	Unit	Standard
Thickness of the rubber panels	10-11	mm	-
Density	1.10	g/cm^3	-
Tensile stress at 2% strain	80	kPa	ASTM D412-16 (ASTM, 2021a)
Tensile strength at 5% strain	180	kPa	ASTM D412-16 (ASTM, 2021a)
Compressive strength at 2% strain	100	kPa	ASTM D575-91 (ASTM, 2018)
Compressive strength at 5% strain	750	kPa	ASTM D575-91 (ASTM, 2018)
Abrasion resistance	81	mm^3	AS 1333 (AS 1333, 2019)
Hardness	60	-	ASTM D2240-15 (ASTM, 2021b)
Young's Modulus	4	MPa	-
Damping factor (ψ) (Gładysiewicz et al., 2019)	0.35	-	-

Table 3. Summary of the experimental program.

Test Number	Axle Load (Tonnes)	Loading Frequency (Hz)	REAG Used	Maximum cyclic stress, $\sigma_{1cyc,max}$ (kPa)	Loading Amplitude, A (kPa)
1	25	15	No	230	100
2	25	15	Yes	230	100
3	25	20	No	230	100
4	25	20	Yes	230	100
5	25	25	No	230	100
6	25	25	Yes	230	100
7	42	10	No	396	183
8	42	10	Yes	396	183
9	42	15	No	396	183
10	42	15	Yes	396	183
11	42	20	No	396	183
12	42	20	Yes	396	183

Table 4. Reduction of lateral displacement and vertical deformation with the inclusion of REAG and the strains mobilized in REAG.

Loading frequency (Hz)	Reduction of lateral displacement (%)		Reduction of vertical deformation (%)		Mobilized strains in REAG (μm/m)			
					25-tonne axle load		42-tonne axle load	
	25-tonne axle load	42-tonne axle load	25-tonne axle load	42-tonne axle load	Parallel to sleeper	Perpendicular to sleeper	Parallel to sleeper	Perpendicular to sleeper
10	-	53.8	-	56.1	-	-	-	-
15	52.1	49.4	60.7	52.3	8086 to 8303	479 to 1062	-	-
20	49.4	44.3	59.7	53.7	13087 to 13432	-495 to -266	20216 to 21131	-59 to 692
25	38.6	-	59.8	-	-	-		-

Table 5. Average reduction of substructure layer stress with the inclusion of REAG.

Location	Average reduction of vertical stress (%)	
	25-tonne axle load	42-tonne axle load
Sleeper-Ballast Interface	4.2	3.2
Ballast-Capping Interface	21.6	11.9
Capping-Subgrade Interface	13.2	9.3
250 mm beneath the Capping-Subgrade Interface	11.3	5.9

List of Figures

Fig. 16. Variation of track settlement at Chullora field tests

Fig. 17. Variation of vertical acceleration of a sleeper at (a) 600^{th}; (b) 3000^{th}; (c) 4800^{th}; and (d) 6000^{th} axle pass

Fig. 18. Measurement of mobilized strains in the REAG during the train passage (500^{th} train pass)

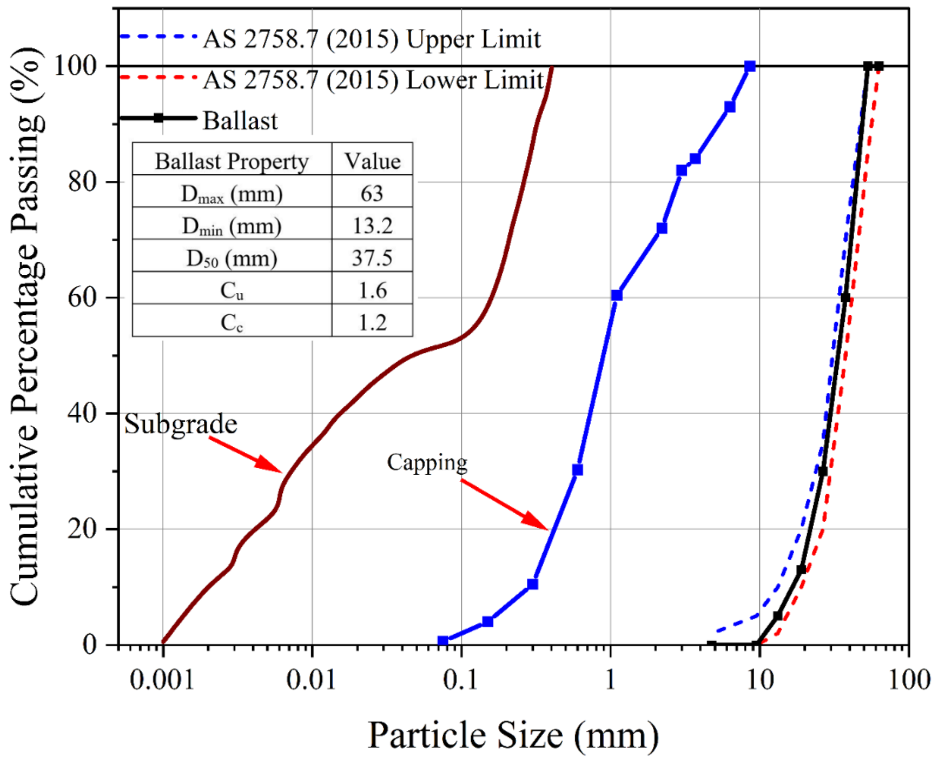

Fig. 1. Particle size distribution of tested materials

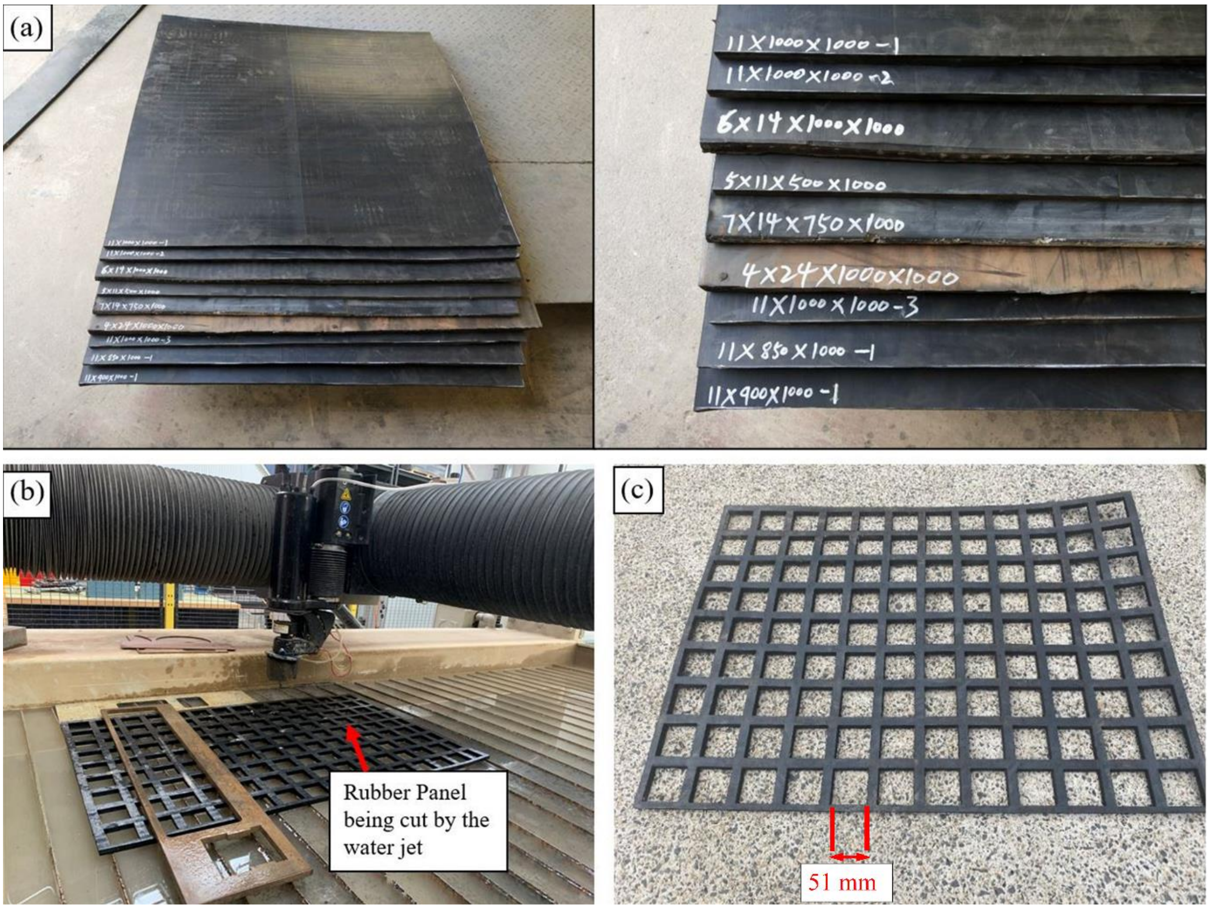

Fig. 2. (a) Rubber sheets derived from discraded conveyor belts (modified from Siddiqui et al., 2023); (b) Rubber panel being cut by the water jet; and (c) a sample REAG used in the test

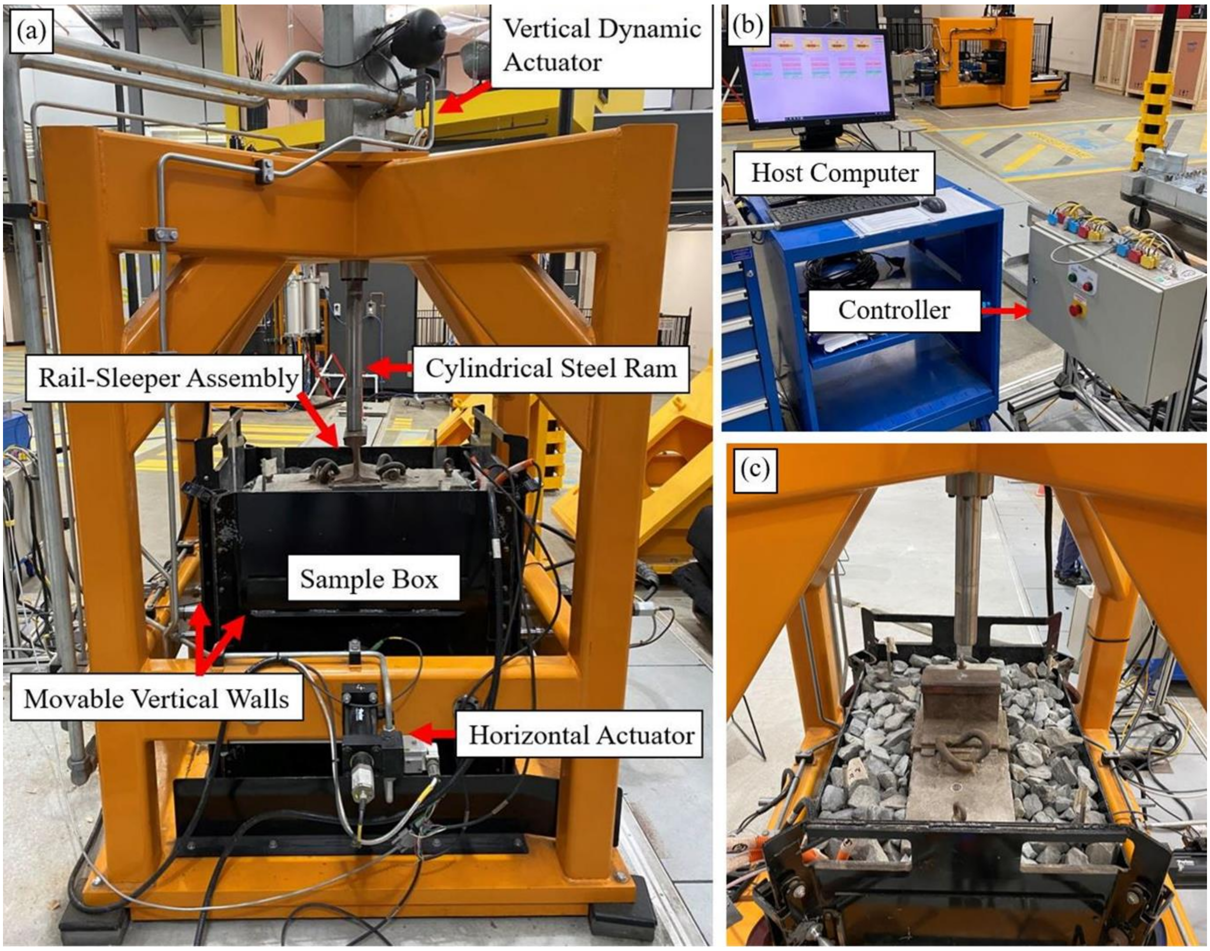

Fig. 3. (a) PSTA; (b) Data logging unit; and (c) Top view of the final specimen arrangement

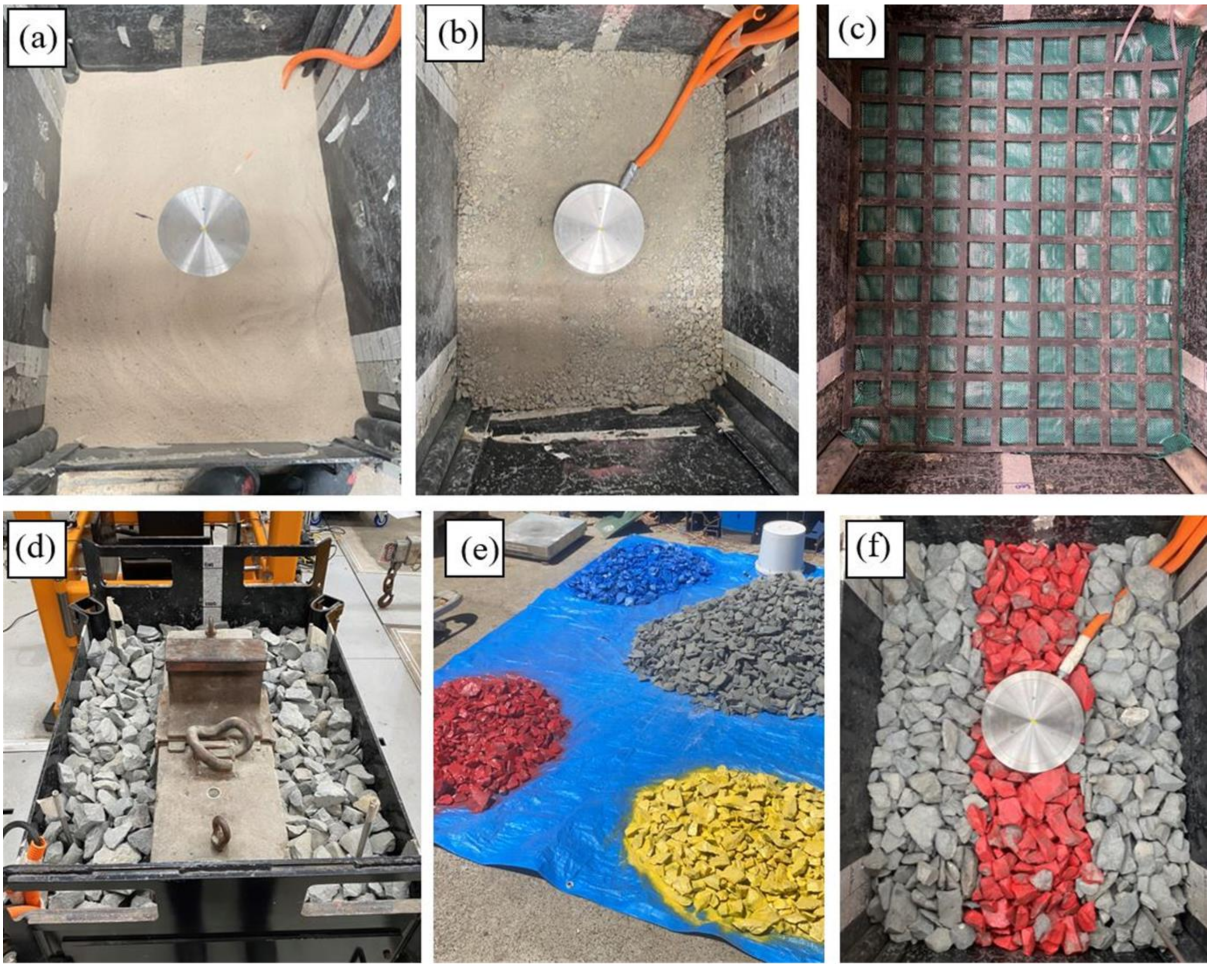

Fig. 4. (a) Pressure cell placed on top of the subgrade layer; (b) Pressure cell placed on top of the capping layer; (c) A layer of REAG placed on top of the woven fabric and capping; (d) Ballast with settlement pegs; (e) Sieved ballast being color coded; and (f) Pressure cell placed on top of the compacted ballast layer.

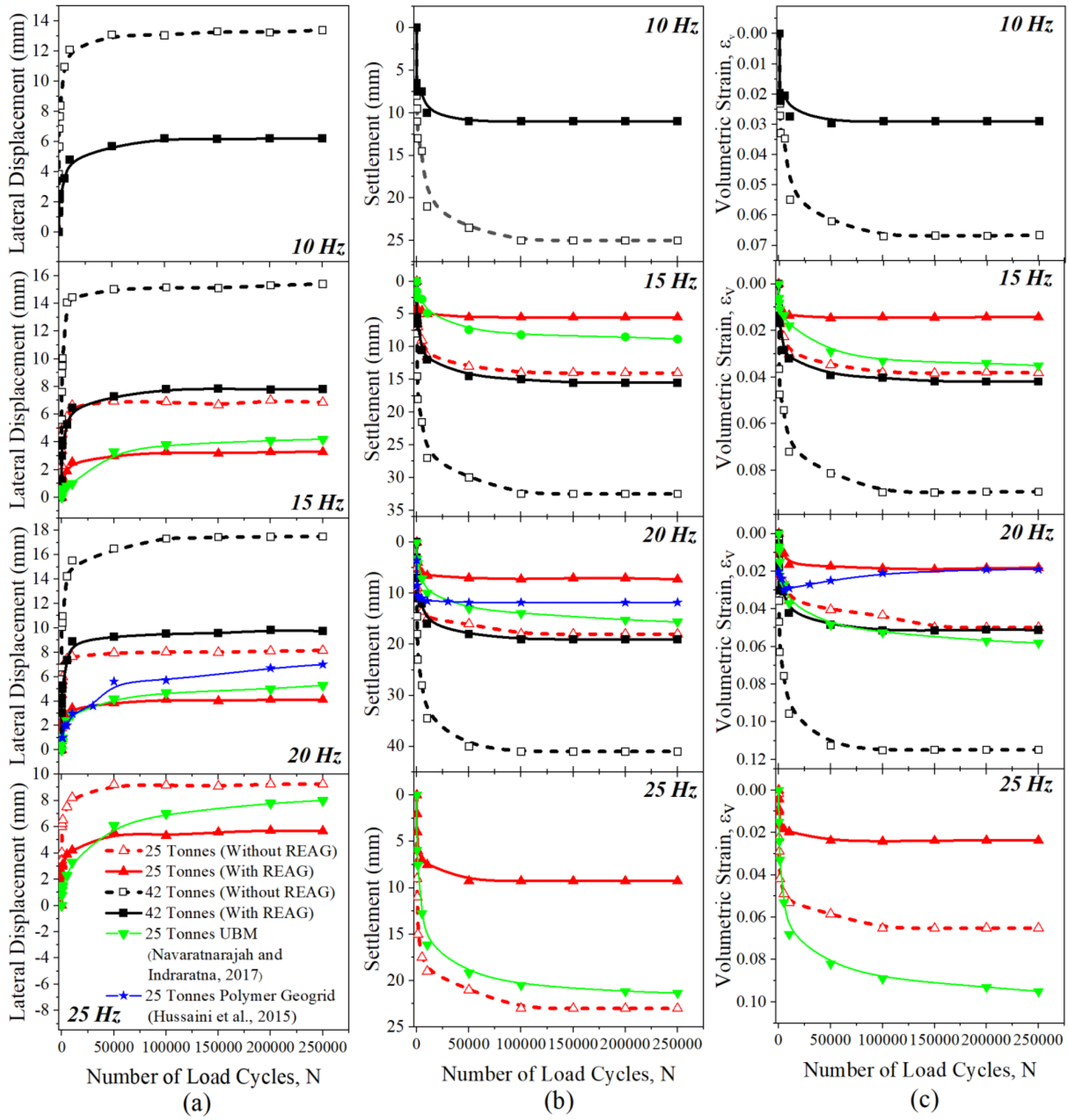

Fig. 5. Measured test results (a) Lateral displacement; (b) Vertical settlement; and (c) Volumetric strain for different loading frequencies at 25-tonne and 42-tonne axle loads

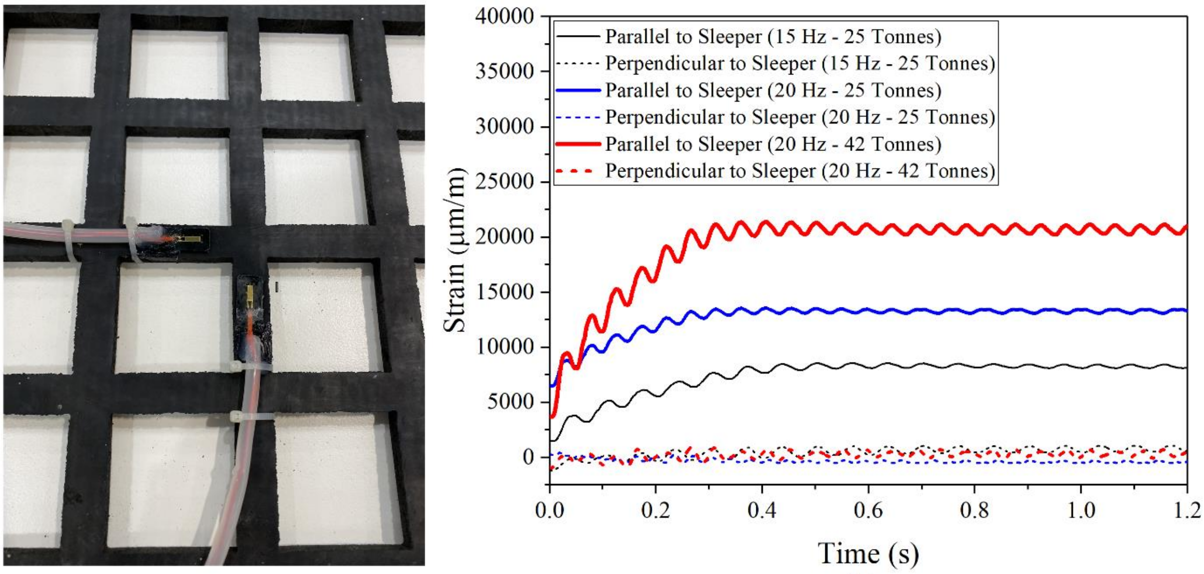

(a) (b)

Fig. 6. (a) Placement of strain gauges on REAG; (b) evolution of mobilized strains in REAG

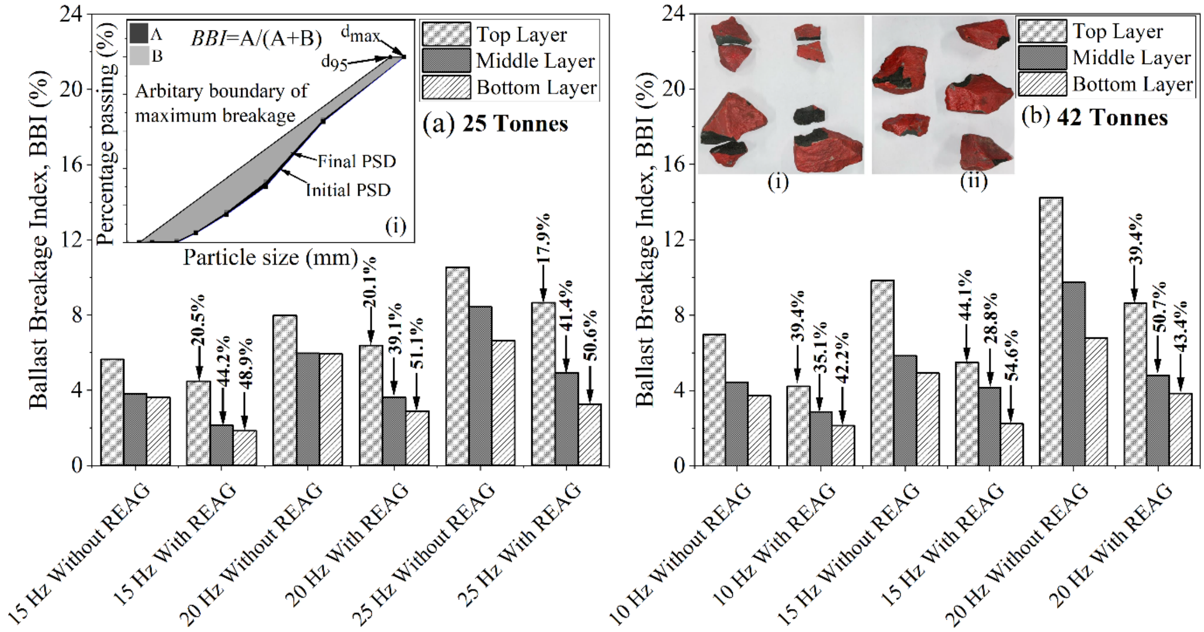

Fig. 7. Measured ballast breakage index (BBI) for different tests: (a) 25-tonne (i. calculation of BBI); and (b) 42-tonne axle load (i. particle splitting; ii. corner breakage)

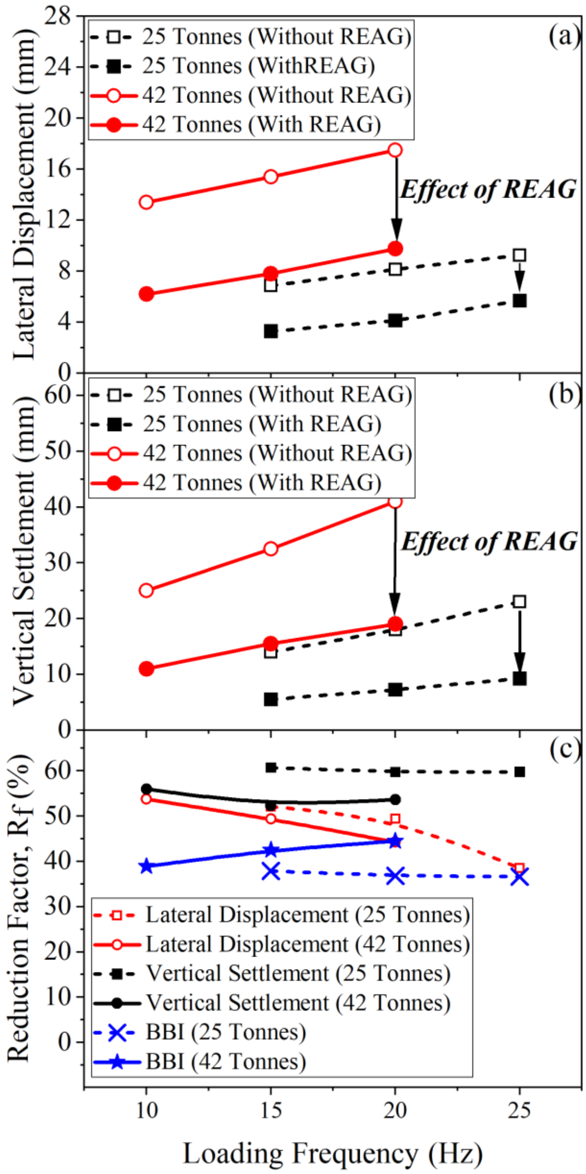

Fig. 8. Influence of loading frequency on: (a) Lateral displacement; (b) Vertical settlement; and (c) Reduction factor, R_f

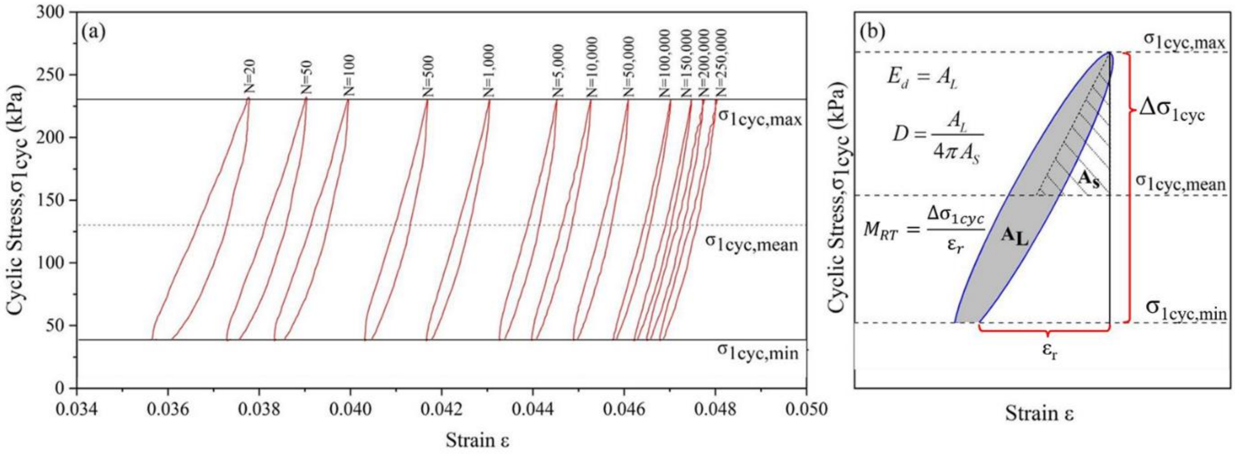

Fig. 9. (a) Typical stress-strain hysteresis loop obtained from cyclic loading tests; (b) schematic of a hysteresis loop showing damping ratio (D), Energy dissipation (E_d) and Resilient track modulus (M_{RT})

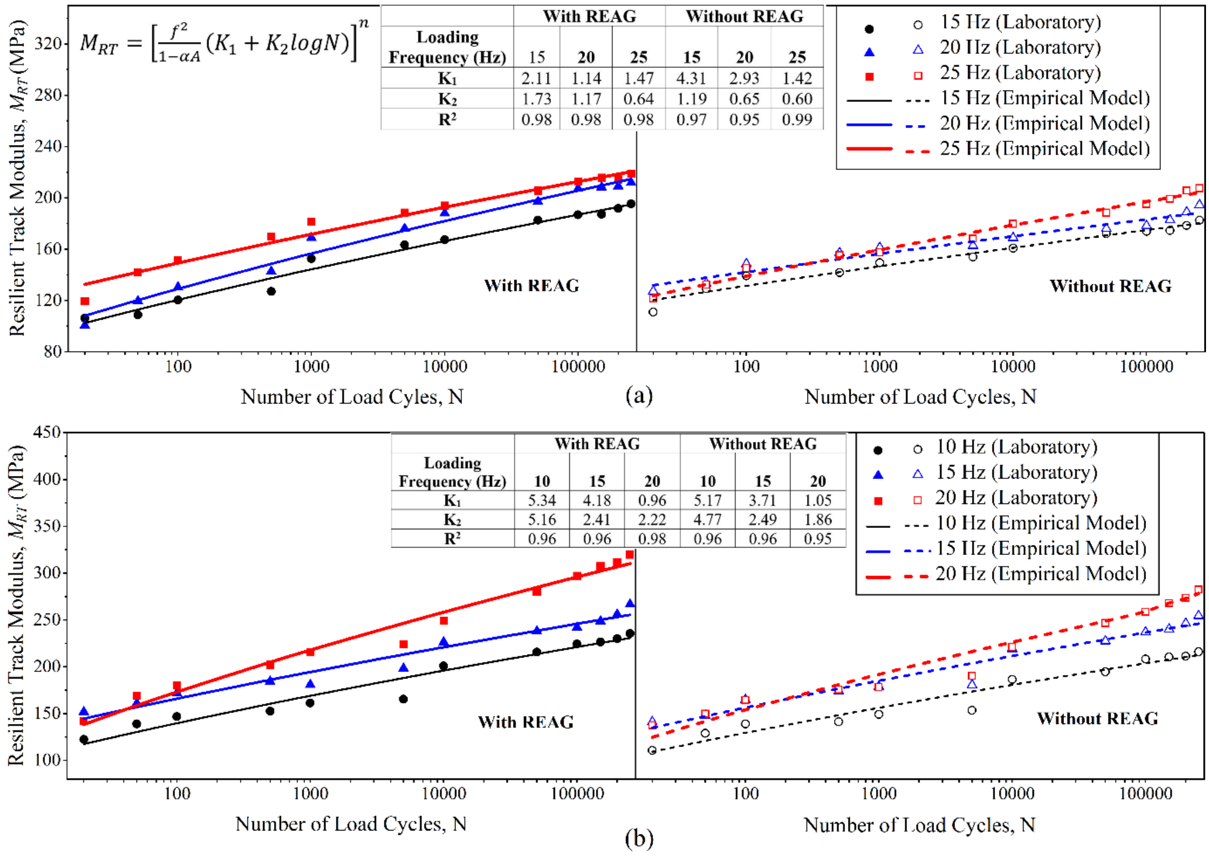

Fig. 10. Variation of resilient track modulus (M_{RT}) for (a) 25-tonne; and (b) 42-tonne axle loads.

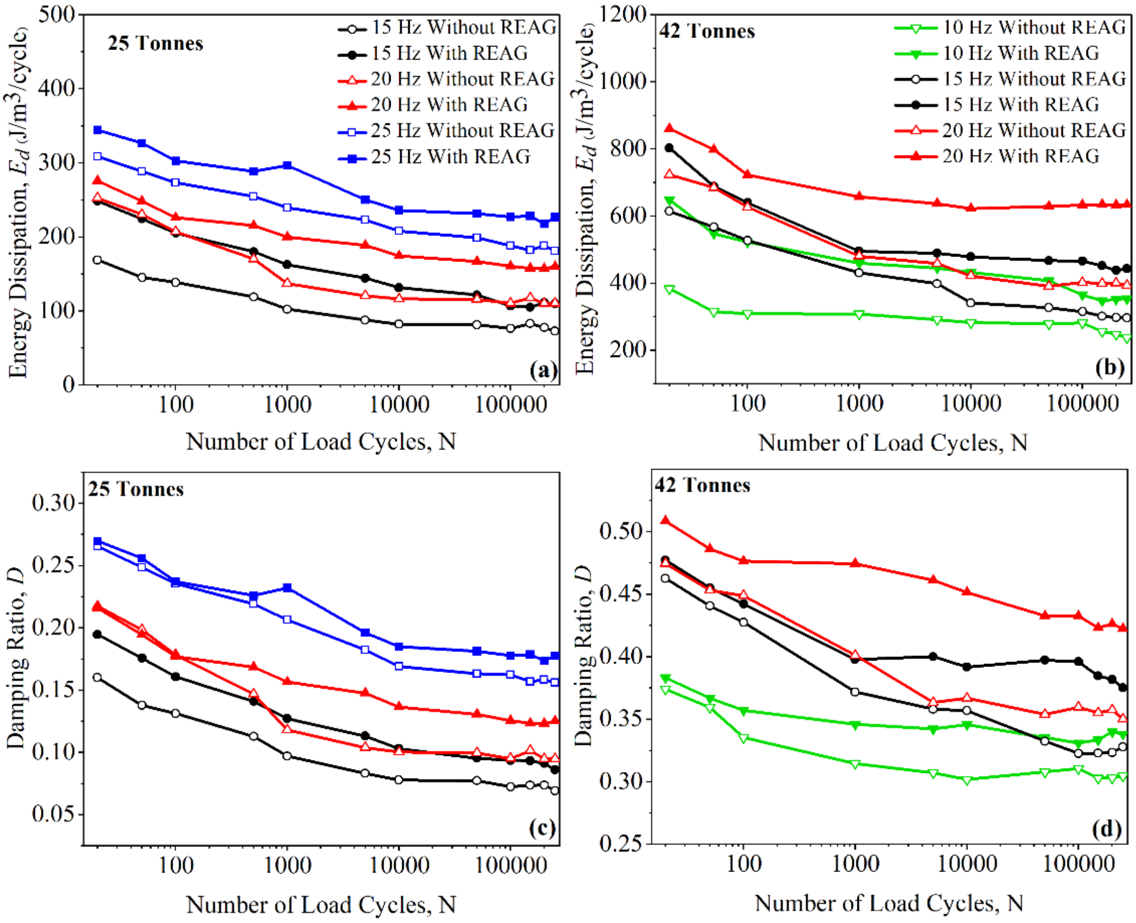

Fig. 11. Variation of energy dissipation (E_d) for (a) 25-tonne; and (b) 42-tonne axle loads; and variation of damping ratio (D) for (c) 25-tonne; and (d) 42-tonne axle loads

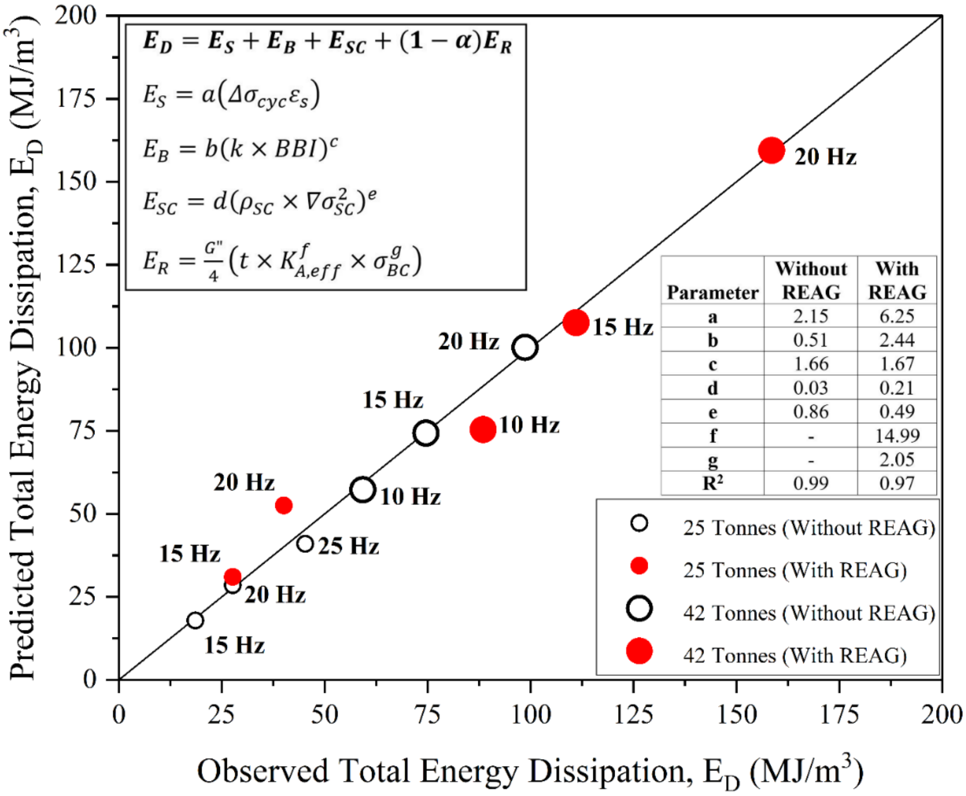

Fig. 12. Predicted and measured values of Total Energy dissipation (E_D)

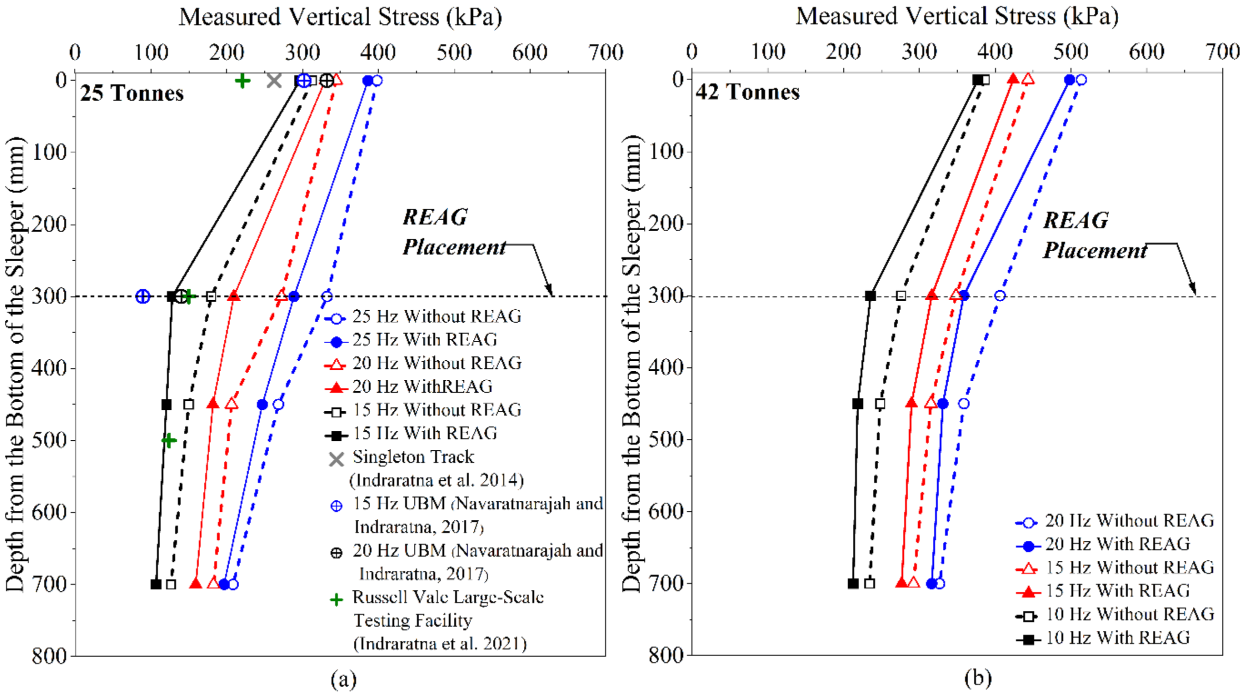

Fig. 13. Variation of vertical stresses within the track substructure: (a) 25-tonne axle load; and (b) 42-tonne axle load

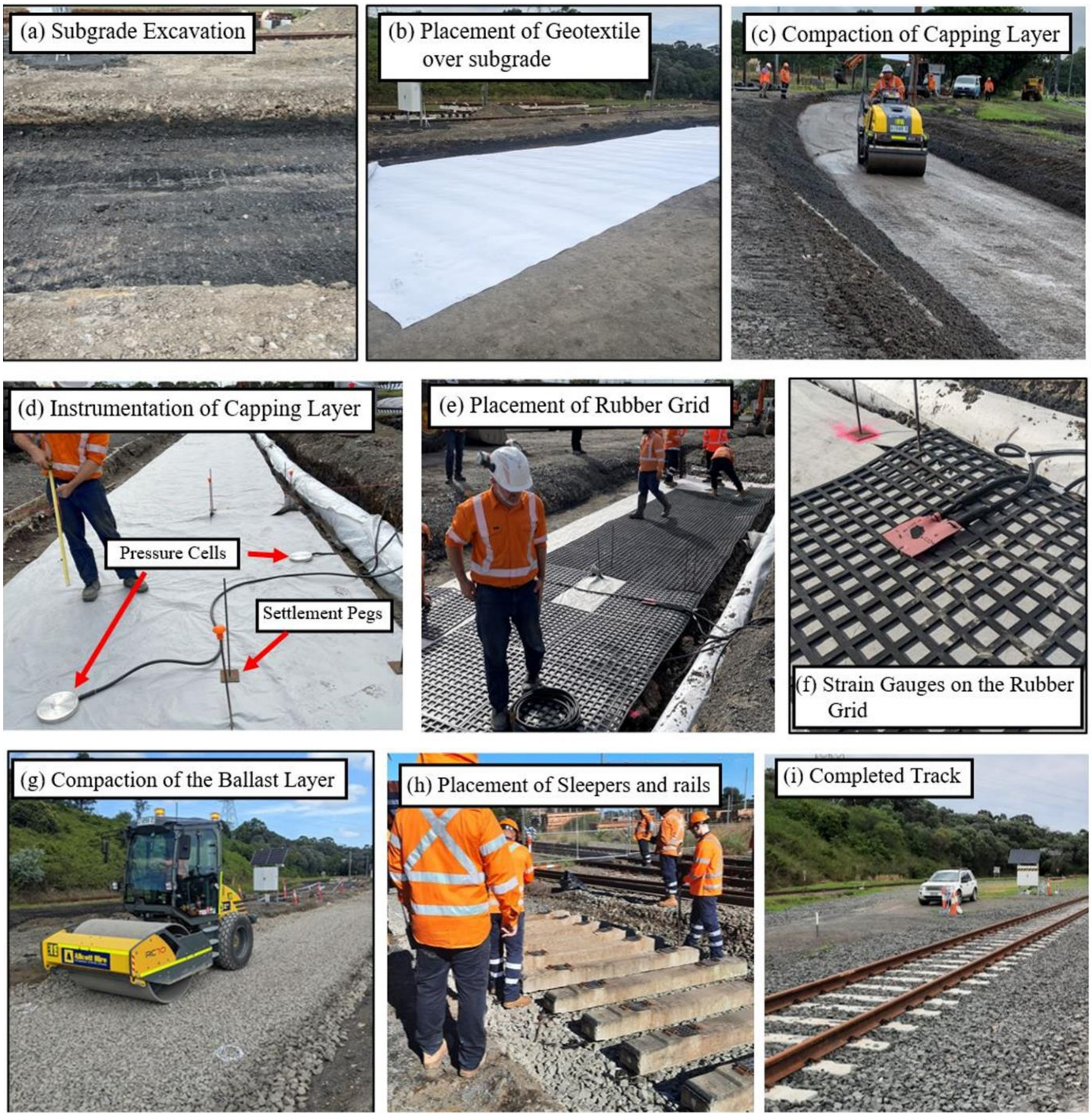

Fig. 14. Stages of track construction at the Chullora Technology Precinct, NSW, Australia

929

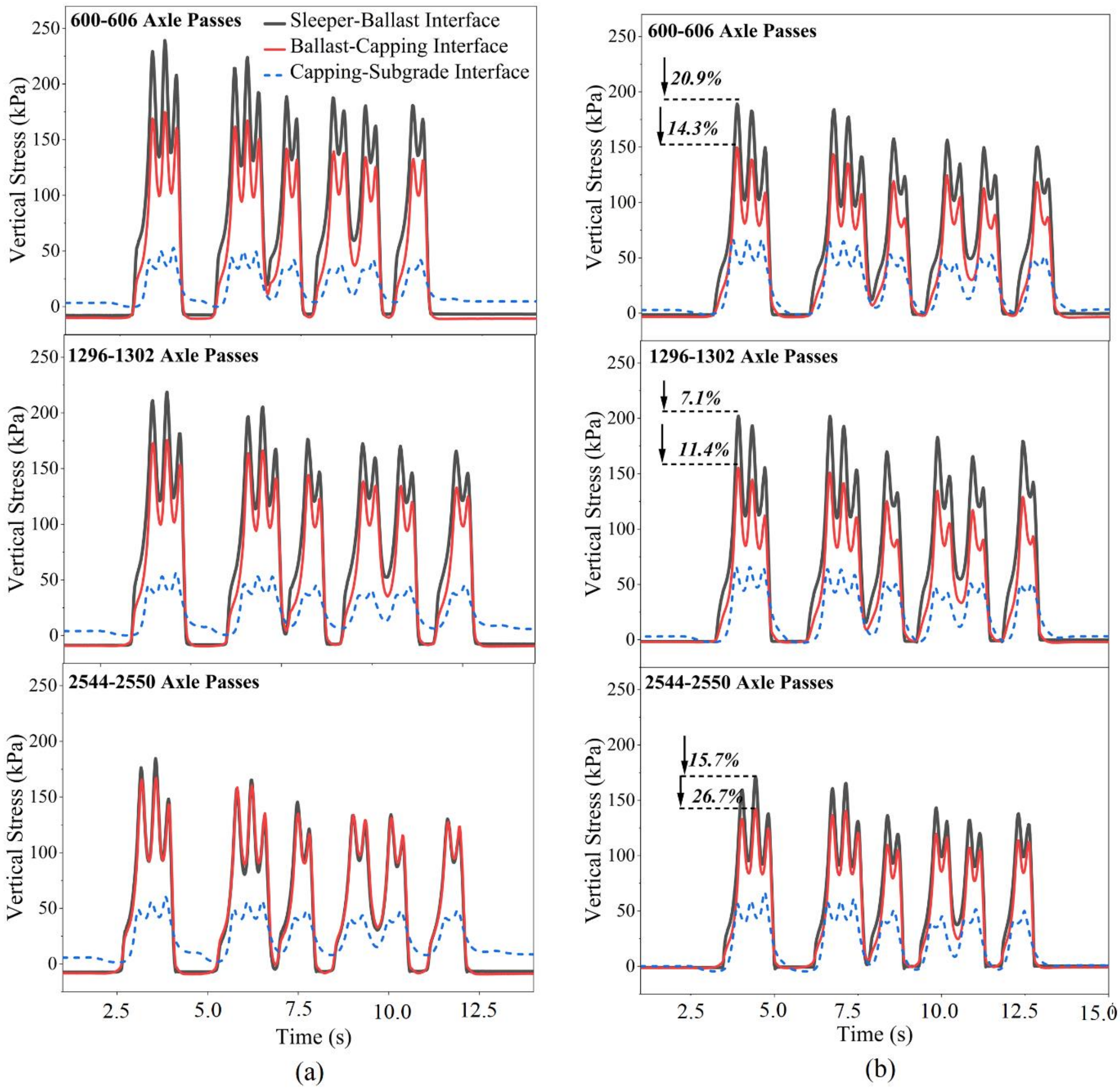

930 **Fig. 15.** Comparison of vertical stress (a) standard track and; (b) REAG track

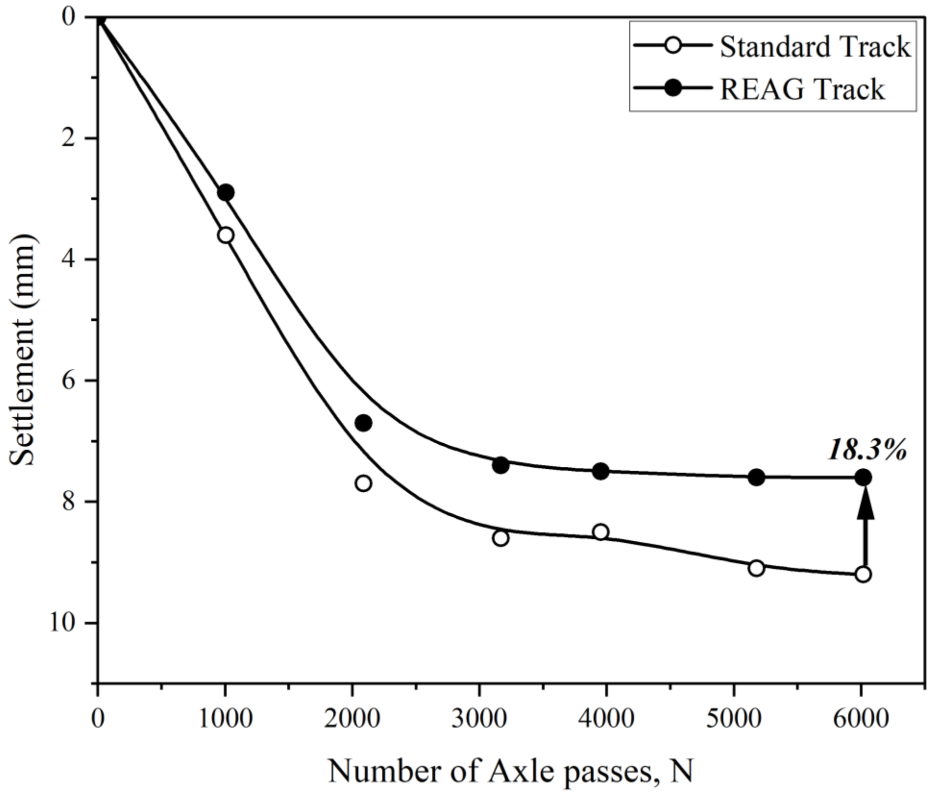

Fig. 16. Variation of track settlement at Chullora field tests

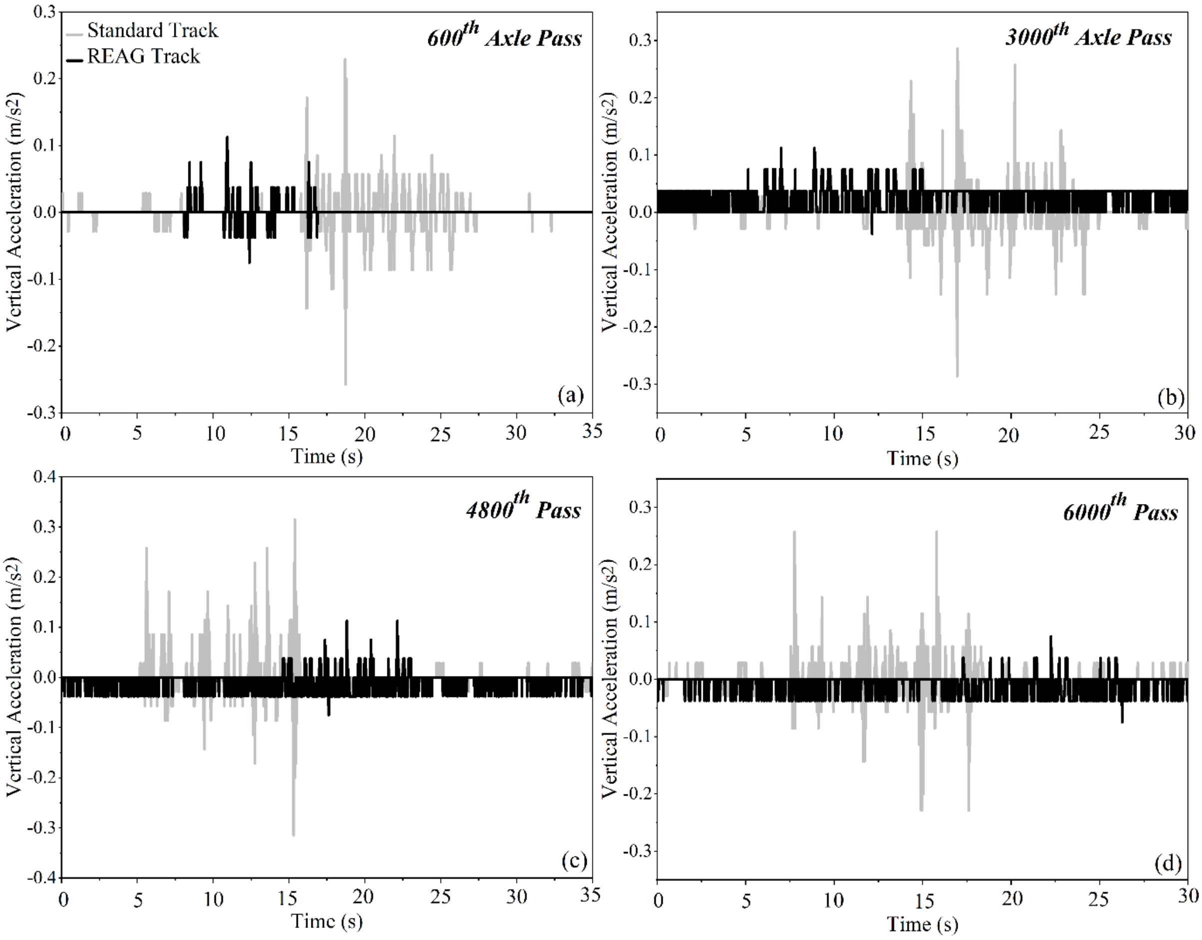

Fig. 17. Variation of vertical acceleration of a sleeper at (a) 600th; (b) 3000th; (c) 4800th; and (d) 6000th axle pass

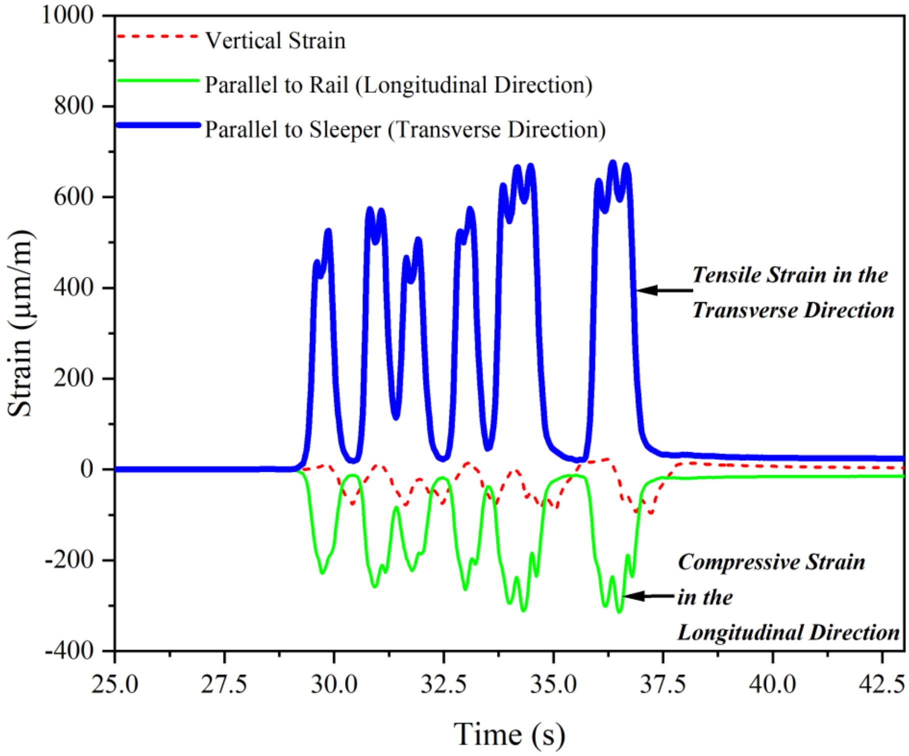

Fig. 18. Measurement of mobilized strains in the REAG during the train passage (500th train pass)